METAL ENRICHED QUASI-ULTRAFINE PARTICLES FROM STAINLESS STEEL GAS METAL ARC WELDING INDUCED GENETIC AND EPIGENETIC ALTERATIONS IN BEAS-2B CELLS

BOUDJEMA J.[1,2], LIMA, B.[1], GRARE C.[1], ALLEMAN L.Y.[3], ROUSSET D.[4], PERDRIX E.[3], ACHOUR D.[1], ANTHERIEU S.[1], PLATEL A.[1], NESSLANY F.[1], LEROYER A.[1], NISSE C.[1], LO GUIDICE J-M.[1,*], GARÇON G.[1,*]

* LGJM and GG contribute equally to this work

[1] CHU Lille, Institut Pasteur de Lille, ULR 4483-IMPacts de l'Environnement Chimique sur la Santé (IMPECS), Univ. Lille, Lille, France

[2] Action Santé Travail, Aix-Noulette, France

[3] IMT Lille Douai, Institut Mines-Télécom, Univ. Lille, Centre for Energy and Environment, F-59000 Lille, France

[4] Institut National de Recherche et de Sécurité (INRS), Department of Pollutant Metrology, 54500 Vandœuvre-lès-Nancy, France

[*] Corresponding author: Guillaume GARÇON, IMPact de l'Environnement Chimique sur la Santé (IMPECS), Institut Pasteur de Lille, CHU Lille, Univ. Lille, Lille, France; E-mail: guillaume.garcon@univ-lille.fr

ABBREVIATIONS

4-HNE: 4-hydroxynonenal
8-OHdG: hydroxy-2'-deoxyguonosine
CCL5: C-C motif chemokine ligand 5
CIRC: international agency for research on cancer
CM-H_2DCFDA: chloromethyl derivative of 2',7'-dichlorodihydrofluorescein diacetate
DRG: differentially regulated gene
DRmiR: differentially regulated miRNA
FC: fold-change
GM-CSF: granulocyte macrophage colony stimulating factor
GMAW: gas metal arc welding
GRO-α: growth-regulated oncogene-α
HAT: histone acetyl transferase
HDAC: histone deacetylase
ICP-MS: inductively coupled plasma-mass spectrometry
IL-1β: interleukin-1 beta
IL-6: interleukin-6
IL-8: interleukin-8
LOQ: Limit of quantitation
MCP-1: monocyte chemoattractant protein 1
miR: miRNA
MMS: methyl methanesulfonate
MS: mild-steel
NF-κB: nuclear factor-kappa B
NRF2: nuclear factor erythroid 2-related factor 2
PM: particulate matter
PTM: post-translational modification
Q-UFP: quasi-ultrafine particles
RANTES: regulated upon activation, normal T cell expressed and presumably secreted
ROS: reactive oxygen species
SS: stainless-steel
t-BHP: tert-Butyl hydroperoxide
TNF-α: tumor necrosis factor
UFP: ultrafine particles
WF: welding fume

ABSTRACT

Recent evidence has supported welding fume (WF)-derived ultrafine particles (UFP) could be the driving force of their adverse health effects. However, UFP have not yet been extensively studied and are currently not included in present air quality standards/guidelines. Here, attention was focused on the underlying genetic and epigenetic mechanisms by which the quasi-UFP (Q-UFP, i.e., ≤ 0.25 µm) of the WF emitted by gas metal arc welding-stainless steel (GMAW-SS) exert their toxicity in human bronchial epithelial BEAS-2B cells. The Q-UFP under study showed a monomodal size distribution in number centered on 104.4 ± 52.3 nm and a zeta potential of -13.8 ± 0.3 mV. They were enriched in Fe > Cr > Mn > Si, and displayed a relatively high intrinsic oxidative potential. Dose-dependent activation of nuclear factor erythroid 2-related factor 2 and nuclear factor-kappa B signaling pathway, glutathione alteration, and DNA, protein and lipid oxidative damage were reported in BEAS-2B cells acutely (1.5 and 9 µg/cm², 24 h) or repeatedly (0.25 and 1.5 µg/cm², 3 x 24 h) exposed to Q-UFP ($p < 0.05$). Alterations of the Histone H3 acetylation were reported for any exposure ($p < 0.05$). Differentially regulated miRNA and mRNA indicated the activation of some critical cell signaling pathways related to oxidative stress, inflammation, and cell cycle deregulation towards apoptosis. Taken together, these results highlighted the urgent need to better evaluate the respective toxicity of the different metals and to include the Q-UFP fraction of WF in current air quality standards/guidelines relevant to the occupational settings.

KEYWORDS: Welding fume; Quasi-ultrafine particles; Metals; human bronchial epithelial BEAS-2B cells; intrinsic oxidative potential; genetic and epigenetic alterations.

INTRODUCTION

Welding is commonly defined as an industrial process where two or more metal pieces are melted together by means of heat to form a join as the parts cool, leading to generation of complex and heterogenous aerosols of metal fumes, gases, and solid particles. Worldwide, an estimated 11 million workers have a job title of welder, and around 110 million additional workers probably incur welding-related exposures. Welding generally involves the exposure to high levels of fine- and ultrafine combustion-derived particulate matter (PM), UV radiation, and electromagnetic fields, and, in some cases, welders are also co-exposed to asbestos and solvents (Guha et al. 2017). In March 2017, a working group met at the International Agency for Research on Cancer (IARC) to evaluate the carcinogenicity of welding. For a majority of the cohort and case-control studies across different countries, time periods, and occupational settings they reported an elevated risk of lung cancer for workers employed as welders or occupationally exposed to welding fume (WF). The risk for lung cancer was higher in welders that had a longer or higher cumulative exposure (i.e., both mild-steel, MS and stainless-steel, SS welding). The working group concluded that there is ‘‘sufficient evidence in humans’’ that WF cause lung cancer and, therefore, classified welding as Group1/carcinogenic to humans (IARC, 2017).

Recent works have identified combustion-derived PM emitted within WF as the driving force of the adverse health effects that occur in humans (Gliga et al. 2017, McCarrick et al. 2019, Pega et al. 2020). While most of this PM mass is found in the fine-sized particle range (i.e., $PM_{2.5}$, aerodynamic diameter $\leq 2.5\mu m$), the largest particle number is in the ultrafine-sized particle range (i.e., $PM_{0.1}$, aerodynamic diameter $\leq 0.1\mu m$). Current health concerns were initially focused on the coarse (i.e., PM_{10}, aerodynamic diameter $\leq 10\mu m$) and fine fractions, mainly because of their ability to migrate deeply and be highly retained down towards the respiratory tract. Emphasis has since then been clearly shifted from larger to ultrafine particles (UFP) (Stone et al. 2017). Epidemiological and toxicological evidence has indeed incriminated their unique properties, compared to those of the larger size particle fractions, including their higher lung deposition, particle number concentration, and surface area per mass. However, the UFP fraction of the WF has not been extensively studied yet and is currently not included in current air quality standards and/or guidelines relevant to the occupational settings, although it probably closely participates for the most part of the human health effects induced by WF (Falcone et al. 2018).

Health effects of WF exposure are complex, as their composition is affected by the type of welding alloy used (Chang et al. 2013; Erdem et al. 2020; Falcon et al. 2018; Leonard et al., 2010; Zheng et al., 2015). Welding involves several processes (e.g., oxyfuel [gas], arc, and resistance welding) and materials (e.g., MS and SS). Arc welding, including one type known as gas metal arc welding (GMAW), in which shielding gases are used to protect against oxidation, is still the most common industrial welding process (Antonini et al. 1999, 2014). This strongest method of joining metals creates a relatively high levels of WF, the composition of which largely depending on whether a MS or a SS electrode is used: GMAW-MS fume contains primarily iron (Fe), zinc (Zn), and manganese (Mn), whereas GMAW-SS fume contains largely Fe, chromium (Cr, also existing in both CrIII and CrVI oxidation states), nickel (Ni), copper (Cu), and Mn (Antonini et al. 2014; Falcone et al. 2018; Ghanem et al. 2021; Stanisławska et al. 2011).

Welding exposures being somewhat complex owing to the diversity of welding processes, a majority of welders generally using multiple welding processes and consumables throughout their lifetime, and some confounders or

additional exposures being possibly regarded in the workplace, associations are still difficult to established (Falcone et al. 2017; Shoeb et al. 2017; Zeidler-Erdely et al. 2010, 2019). All the cellular and/or molecular underlying mechanisms responsible for the toxicity and even the carcinogenicity of WF are still not fully understood. Therefore, controlled experimental studies are crucial to better understand which WF type and which of their metal components are the most toxic and have the greatest carcinogenic potential. Series of animal studies, by which the exposure to WF was well-controlled, were undertaken to better elucidate the role of WF metal composition (e.g., SS versus MS) on lung toxicity and cancer development. Some of them reported oxidative stress conditions, inflammatory responses, and immune suppression (Falcone et al. 2018; Gliga et al. 2017; Grigg et al. 2017; Marongiu et al. 2016; McCarrick et al. 2019; Pega et al. 2020; Stanisławska et al. 2020). In a two-stage initiation-promotion model of lung carcinogenesis, GMAW-SS fume significantly increased lung tumor multiplicity after both an oropharyngeal aspiration and inhalation exposure in A/J mice (Falcone et al. 2017; Zeidler-Erdely et al., 2010). An *in vivo* study indicated that WF derived from SS welding acted as a tumor promoter and lead to lung cancer in mice initially exposed to 3-methylcholanthrene (Zeidler-Erdely et al. 2013). Further demonstration of the greater toxic effect of GMAW-SS fume than GMAW-MS fume was reported in other animal models. For example, Antonini et al. (2007, 2009) found that GMAW-MS fume caused no lung inflammation or lung injury in Sprague-Dawley rats 1, 4, or 11 days post-inhalation compared to GMAW-SS fume, which caused significant lung damage. Regardless, in vivo studies investigating exposures to WF as occurring in GMAW-MS or -SS are still lacking to contribute to an entire knowledge of the metal components closely responsible for their toxicity and/or their carcinogenicity. Two main topics that need to be further evaluated in future experimental models are not only the contribution of their individual chemicals and/or the specific roles of their UFP fraction in the development of lung toxicity and tumor formation, but also the cellular and molecular underlying mechanisms by which they contribute to cause lung toxicity and even lung tumorigenesis.

The better knowledge of the cellular and molecular underlying mechanisms involved in the pathogenicity of lung toxicity and even lung cancers related to WF exposure is still essential and could notably rely on relevant lung cell culture models (Leclercq et al., 2016). Indeed, clinical and basic science applications have focused on the bronchial epithelium because of the chronic inflammatory diseases resulting from disruption of this region (Boublil et al., 2013; Leclercq et al. 2017a). Up to now, only very few in vitro studies have been undertaken to better elucidate the individual chemicals and/or UFP sized-fractions of WF and their critical roles in the harmful health effects they induced.

As supported by the current literature, the underlying mechanism of post-inflammatory effects of WF is certainly mostly launched by soluble intermediate metals through the excessive production of reactive oxygen species (ROS) (Ghanem et al. 2021; Stanislawaka et al. 2020). One of the most well-described toxicological mechanisms responsible for the lung adverse effects of combustion derived-PM is the pro-inflammatory response driven by oxidative stress (Abbas et al. 2019; Badran et al. 2020a; Cazier et al. 2016; Garçon et al. 2001, 2006; Leclercq et al. 2018; Saint-Georges et al. 2008; Sotty et al. 2020). Of course, ROS generation and pro-inflammatory reaction have been reported among welders who are exposed to high levels of PM emitted within WF, but other underlying mechanisms, not even fully elucidated, like critical epigenetic alterations, could probably interplay to

induce the adverse health effects. New toxicological research is therefore urgently requested to improve the current knowledge about the specific role of the UFP fraction in the overall toxicity of WF.

Hence, in this work, we sought to better evaluate the toxicity of the quasi-UFP fraction (Q-UFP, i.e., $PM_{0.25}$) of the WF emitted by GMAW-SS in human bronchial epithelial cells (BEAS-2B). Firstly, we aimed to physically and chemically characterize this Q-UFP fraction. Secondly, attention was focused on the ability of this Q-UFP fraction to induce cytotoxicity, pro-oxidative and/or pro-inflammatory responses, genetic and/or epigenetic alterations, and, therefore, some related cell signaling pathway activation in BEAS-2B cells acutely or repeatedly exposed. These relevant results will also contribute to new insights of the critical role played by the Q-UFP fraction in human adverse effects induced by the exposure to GMAW-SS-derived WF.

MATERIALS AND METHODS

Chemicals

Merck-Millipore (St Quentin-en-Yvelines, France) provided BEAS-2B cells (ATCC® CRL-9609™), cOmplete™, EDTA-free Protease Inhibitor Cocktail, Phosphatase Inhibitor Cocktail, RIPA buffer, CHAPS buffer, MILLIPLEX® MAP human cytokine/chemokine magnetic bead panel-immunology multiplex assays, methyl methanesulfonate (MMS), and all the other chemicals. ThermoFisher scientific (Villebon-sur-Yvette, France) provided collagen type I from rat tail, chloromethyl derivative of 2',7'-dichlorodihydrofluorescein diacetate (CM-H_2DCFDA), Pierce™ BCA protein assay kits, Single-channel dead cell apoptosis kits with Annexin V alexa fluor™ 488, and SYTOX™ green dyes, and all the other reagents for chemistry, and cellular and molecular biology. Qiagen (Courtaboeuf, France) provided RNeasy mini Kits. Promega (Charbonnière-les-Bains, France) provided CellTiter-Glo® luminescent cell viability, GSH/GSSG-Glo™ assay, and Caspase Glo® 3/7, Caspase Glo® 8, and Caspase Glo® 9 assays. Abcam (Cambridge, UK) provided 4-hydroxynonenal (4-HNE) modified bovine serum albumin, rabbit polyclonal anti-4-HNE antibody, and Protein carbonyl content assay kit, and 8-hydroxy-2'-deoxyguonosine (8OHdG) ELISA kit. Active Motif (La Hulpe, Belgium) provided Nuclear extract and TransAM® nuclear factor erythroid 2-related factor 2 (NRF2) and nuclear factor-kappa B (NF-κB) kits, Global DNA Methylation LINE-1 Assay, Histone Purification Mini Kit, Histone total H3, H3K9ac, and H3K27ac ELISA kits, and histone acetyl transferase (HAT) and histone deacetylase (HDAC) Assay kits. Bio-Techne (Lille, France) provided repair endonuclease hOGG1.

Collection of WF particles

WF particles were produced according to GMAW-SS process using an automatic welding bench as described elsewhere (Bonthoux et al. 2016). The bench is equipped with a Digiwave welding installation (SAF-FRO, Le Grand Quevilly, France) using M21 as shielding gas (i.e., 82% Ar / 18% CO_2). Briefly, a stainless-steel plate (750 x 50 x 6 mm) moves under the torch feeded with a SS wire (Filinox 316LSi 1 mm in diameter, SAF-FRO) to produce a regular weld bead. All the fumes are drawn into an extraction hood under a flow rate of 120 m^3/h. A sampling probe inside the duct was connected to a 4-way flow splitter (Palas Gmbh, Karlsruhe, Germany) linked to the sampling devices. The total sampling flow rate ranged between 36.8 and 37.8 L/min according to the sampling configuration. For this study, several Sioutas cascade impactors (SKC Ltd, Blandford Forum, United-Kingdom) were used to collect particles based on their aerodynamic diameter over 5 stages (< 0.25 µm, 0.25 - 0.50 µm, 0.50 - 1 µm, 1 - 2.5 µm, > 2.5 µm). A SG10-2 pump (GSA Germany Gmbh, Frankfurt am Main, Germany) was used to maintain the sampling flow rate of 9 L/min. Polycarbonate (PC) filters with 25-mm diameter and 0.8 µm pore size (Whatman, Kent, United-Kingdom) were used as the impaction media. The finest particles (i.e. also called Q-UFP, aerodynamic diameter ≤ 0.25 µm) were collected on a 37-mm diameter and 0.8 µm pore size PC filters (Whatman) placed onto a 37-mm cellulose pad to prevent any leakage. Generations of WF were repeated following the exact same procedure until getting sufficient mass. For each generation, a way of the flow splitter was dedicated to real time monitoring of

number concentration and size distribution determined with an electrical low-pressure impactor ELPI$^+$ (Dekati, Kangasal, Finland).

Determination of the mass of the collected WF particles

The mass concentration of particles collected on the PC filters was measured gravimetrically using a XP2U Ultra Micro balance (Mettler-Toledo, Viroflay, France) placed in a particle-controlled room. After storage in the room atmosphere for at least 12 h, filters were weighed before and after aerosol sampling. Static charges were discharged using an anti-static ionizing bar (Elcowa SA, Mulhouse, France). The mass of the collected particles was calculated by difference and corrected with field blank filters to adjust for humidity and temperature-related variations. Limits of quantitation (LOQ) were below 30 µg and 75 µg for 25 mm and 37 mm PC filters, respectively.

Extraction of WF particles

The samples of WF collected on weighed PC filters were water-extracted in a clean room with an ultrasound system (Vibracell 75455, 500W, 20 KHz) equipped with cold circulating water. Three successive MilliQ water baths were used and combined before being distributed among the different teams. The Q-UFP fraction accumulated from WF emissions (100.9 mg in 50 mL of MilliQ water) was stored at -20°C until its further use for the physical and chemical characterization and the toxicological study.

Physical and chemical characterization of WF-derived Q-UFP

The size distribution and the zeta potential of the Q-UFP fraction of the WF emitted by GMAW-SS process were studied using a Zetasizer Nano ZSP™ (Malvern Instruments SARL, Orsay, France) after a sonication (45W, 40 kHz, 2 min) with a Branson Sonifier SFX 150 (ThermoFisher Scientific).

The metal composition of the Q-UFP was studied by inductively coupled plasma-mass spectrometry (ICP-MS, Perkin Elmer NeXion 300X, Perkin Elmer, Villebon-sur-Yvette, France). The Q-UFP suspension was weighed and quantitatively mineralized in an acidic medium (HNO_3/H_2O_2/HF) at 220°C in a microwave oven (Ultrawave, ThermoFisher scientific). According to Mbengue et al. (2014) and Leclercq et al. (2017b), the analyses were carried out in triplicates for three sub-samples of 100 µg of Q-UFP and for two different dilutions (i.e., 1/2 and 1/10). Repeated measurements of blanks and quality control (QC) standards attached to the NIST were performed during each analytical run. A mixed internal standard (^{69}Ga, ^{103}Rh) was added (1µg/L) to each analyzed solution to correct for the drift of the ICP-MS signal. Moreover, in order to validate the extraction procedure, several samples (~ 1 mg) of NIST SRM 1648a (i.e., Urban particulate matter, NIST, Gaithersburg, MAa, USA) were systematically tested as standard reference material. Thirty trace elements and 7 major elements were determined: Ag, As, Ba, Be, Bi, Cd, Ce, Co, Cr, Cs, Cu, La, Li, Mn, Mo, Ni, Pb, Pd, Pt, Rb, Sb, Se, Sn, Sr, Th, Ti, Tl, U, V, Zn, Al, Ca, Fe, K, Mg, Na, and Si.

During 7 experiments, WF were collected for hexavalent chromium (CrVI) determination in a Millipore® cassette (opening diameter 4 mm) fitted with a 37 mm quartz fiber filter (QMA, Whatman) impregnated with magnesium sulfate and sodium carbonate. The CrVI was determined by ion chromatography (Dionex, ThermoFisher

scientific) after extraction in a Na_2CO_3/NaOH solution with the one extraction protocol Métropol M-43 (INERIS, 2020).

Intrinsic oxidative potential of WF-derived Q-UFP

The intrinsic oxidative potential (OP) of WF-derived Q-UFP was determined through CM-H_2DCFDA acellular assay and glutathione oxidation (i.e., ratio between oxidized form and reduced form, GSSG/GSH), according to Crobeddu et al. (2020). Briefly, for CM-H_2DCFDA acellular assay, ROS-produced by Q-UFP, ranging from 10 to 100 µg/mL, convert the non-fluorescent CM-H_2DCFDA probe (20 µM) into the fluorescent 2′,7′-dichlorofluorescein (DCF). Fluorescence generated by probe oxidation was kinetically monitored for 30 min at λ_{ex} = 485 nm and λ_{em} = 520 nm, at 37 °C, with Spark® 10M multimode plate reader (TECAN France SASU, Lyon, France). For glutathione status, Q-UFP from 10 to 100 µg/mL were incubated for 4 h at 37 °C in a solution containing physiological concentrations (200 µM) of GSH in PBS at pH 7.4 with constant mixing. After incubation, both the GSH and GSSG concentrations, and also the glutathione status, were evaluated thanks to the GSH/GSSG-Glo™ assay (Promega). Hydrogen peroxide (H_2O_2) at 100 µM was used as positive control.

Cell culture and exposure to WF-derived Q-UFP

Normal human bronchial epithelial BEAS-2B cells (ATCC® CRL-9609™), which derived from normal human bronchial epithelial cells obtained from autopsy of non-cancerous individual, were cultured as published elsewhere (Badran et al. 2020b, Leclercq et al. 2017, Sotty et al. 2020). Briefly, depending on the toxicological endpoints under study, BEAS-2B cells were cultured in 95 % humidified air with 5 % CO_2 at 37°C in 75 cm² CellBIND® surface plastic flasks (Corning; Sigma-Aldrich), in LHC-9 serum-free medium supplemented with 1% (v/v) penicillin (10,000 U/mL)-streptomycin (10,000 µg/mL) solution (ThermoFisher Scientific) once cells had reached 80 % of confluence. Thereafter, BEAS-2B cells were seeded for 24 h at 25,000 cells/well on 96-well CellBIND® surface plastic microplates coated with collagen type I from rat tail (0.03 mg/mL) or at 200,000 cells/well on 6-well CellBIND® surface plastic microplates coated with collagen type I from rat tail (0.03 mg/mL), in LHC-9 serum-free medium supplemented with 1% (v/v) penicillin (10,000 U/mL)-streptomycin (10,000 µg/mL) solution, and 2% (v/v) amphotericin B solution (20 µg/mL) (ThermoFisher Scientific). Immediately prior the exposure, WF-derived Q-UFP solution (i.e., 1.91 µg/µl) was diluted in sterile HBSS supplemented with amphotericin B solution (20 µg/mL) at 2 % (v/v) in order to obtained final concentrations ranging from 0.33 ng/µL (i.e., 0.1 µg/cm²) to 165 ng/µL (i.e., 50 µg/cm²), and sonicated for 2 x 1 min. Thereafter, for cytotoxicity, BEAS-2B cells were exposed one or three times, for 24 h, as negative controls (i.e., sterile HBSS supplemented with 2 % v/v amphotericin B) or Q-UFP-exposed cells (i.e., concentrations ranging from 0.1 to 50 µg Q-UFP/cm², suspended in sterile HBSS supplemented with 2 % v/v amphotericin B). For the Comet assay, cells were seeded at a density of 150,000 to 400,000 cells/well in LHC-9 in 6-well CellBIND® surface plastic microplates coated with collagen type I from rat tail (0.03 mg/mL) in LHC-9 serum-free medium supplemented with 1 % (v/v) penicillin (10,000 U/mL)-streptomycin (10,000 µg/mL) solution and 2% (v/v) amphotericin B solution (20 µg/mL), prior to BEAS-2B cell exposure, acutely (i.e., 1 time for 4 h or 24 h) or repeatedly (i.e., 3 times for 24 h) to WF-derived Q-UFP. For all the other toxicological endpoints, BEAS-2B cells

were exposed one or three times, for 24 h, as negative controls (i.e., sterile HBSS supplemented with 2 % v/v amphotericin B solution) or Q-UFP-exposed cells (i.e., at two concentrations: calculated lethal dose at 10%, LD_{10}, and 6 x DL_{10}, suspended in sterile HBSS supplemented with 2 % v/v amphotericin B solution). Hydrogen peroxide (H_2O_2, 100µM), tert-Butyl hydroperoxide (t-BHP, 10 µM), lipopolysaccharide (LPS) from E. coli (50 µg/mL), methyl methanesulfonate (MMS, 10 or 15 µg/mL), or staurosporin (1 µM) served as positive controls. Twenty-four hours later, 1 mL-aliquots of cell-free culture media were sampled and quickly frozen at -80°C. Adherent cells were washed once with 1mL-aliquots of cold sterile PBS, and either quickly fixed or quickly frozen at -80°C. For mRNA and miRNA analyses, adherent cells were washed once with 1mL-aliquots of cold sterile PBS and thereafter lysed with 700 µL of QIAzol lysis buffer and quickly frozen at -80°C.

WF-derived Q-UFP-induced cytotoxicity

Intracellular ATP concentrations of BEAS-2B cells were determined using the CellTiter-Glo® luminescent cell viability (Promega).

WF-derived Q-UFP-induced other toxicological endpoints

The further study of the toxicological endpoints needed the preparation of different cell lysates: (i) nuclear factor erythroid 2-related factor 2 (NRF2) DNA binding activity binding activity, nuclear factor-kappa B (NFκB) DNA binding activity, histone H3 post-translational modifications (PTM), and caspase activities were studied after cell lysis with RIPA buffer supplemented with cOmplete™EDTA-free Protease Inhibitor Cocktail and Phosphatase Inhibitor Cocktail (Merck-Millipore), (ii) 8-OHdG and global DNA methylation were studied after DNA extraction with the QIAamp DNA Mini Kit (Qiagen), (iii) histone acetyl transferase (HAT) and histone deacetylase (HDAC) activities were studied after cell lysis with CHAPS buffer (Merck-Millipore), and (iv) mRNA and miRNA expression profiles were studied after total RNA extraction with the miRNeasy Mini Kit (Qiagen).

ROS production and oxidative damage: Firstly, the fluorescence of CM-H_2DCFDA (1 µM) was kinetically monitored at 37°C within BEAS-2B cells (Sotty et al. 2020). Secondly, the NRF2 DNA binding activity was studied using TransAM® NRF2 from Active Motif. Associated gene expressions of some members of the NRF2 signaling pathway (i.e., *heme oxygenase 1, HMOX, and NAD(P)H quinone dehydrogenase 1, NQO1*) were evaluated by RT-qPCR using specific Taqman™ gene expression assays (*HMOX*: Hs01110250_m1, *NQO1*: Hs01045993_g1, *and RNA18S*: Hs99999901_s1), a StepOnePlus™ Real-Time PCR System, and the Expression Suite Software (ThermoFisher scientific). Thirdly, the concentrations of 4-hydroxynonenal (4-HNE), carbonylated protein (CO-protein), 8-hydroxy-2'-deoxyguanosine (8-OHdG), and glutathione were studied respectively thanks to a home-made competitive ELISA, based on MSD technologies (Mesoscale Discovery, Rockville, MD, USA), using 4-HNE-modified BSA and rabbit polyclonal anti-4-HNE antibody (Abcam), Protein carbonyl content assay kits (Abcam), 8-hydroxy-2'-deoxyguanosine ELISA kit (Cell Biolabs, and GSH/GSSG-Glo™ assay (Promega), as published elsewhere (Anthérieu et al. 2017; Garçon et al. 2000; Leclercq et al. 2016). Hydrogen peroxide (i.e., H_2O_2, 100 µM, 4 h)-treated BEAS-2B cells served as positive controls.

Cytokine and chemokine secretion: The NF-κB DNA binding activity was studied using TransAM® NF-κB from Active Motif. The secretion of C-C motif chemokine ligand 5 (CCL5) or regulated upon activation, normal T cell expressed and presumably secreted (RANTES), granulocyte macrophage colony stimulating factor (GM-CSF), growth-regulated oncogene-α (GRO-α), interleukin-1 beta (IL-1β), interleukin-6 (IL-6), interleukin-8 (IL-8), monocyte chemoattractant protein 1 (MCP-1), and tumor necrosis factor (TNF-α), in the cell-free culture supernatants of BEAS-2B cells was detected by MILLIPLEX® MAP Human Cytokine/Chemokine Magnetic Bead Panel-Immunology Multiplex Assay (Merck-Millipore) (Devos et al. 2019). Lipopolysaccharide (LPS from E. coli, 50 µg/mL, 24 h)-treated BEAS-2B cells served as a positive control.

Genetic alterations: The comet assay was performed under alkaline conditions (pH > 13) in compliance with a. previously described protocol (Singh et al., 1988; Tice et al., 2000; Witte et al., 2007). Slight modifications using the repair endonuclease hOGG1 (R&D systems, Minneapolis, USA) were carried out to detect specifically oxidative DNA damage, based on Collins' and Smith's procedures (Collins et al. 1993; Smith et al., 2006). For each group, 4 duplicate slides per culture were prepared (i.e., 2 slides for the standard comet assay and 2 slides for the hOGG1-modified comet assay). When scoring for DNA migration, slides were independently coded and analyzed after the addition of 25 µL of propidium iodide at 20 µg/mL and a coverslip. Slides were then examined at 250 X magnification using a fluorescence microscope (Leica Microsystems SAS - DM 2000, Heerbrugg, Switzerland) equipped with an excitation filter of 515-560 nm and a 590 nm barrier filter, connected through a gated monochrome CCD IEEE1394 FireWire video camera (Allied Vision Technologies) to the Comet Assay IV Image Analysis System, version 4.11 (Perceptive Instruments Ltd, Suffolk, United Kingdom). One hundred randomly selected cells per slide were scored. DNA damage was expressed as percentage of DNA in the tail (% tail intensity) (Burlinson et al., 2007; Lovell and Omori, 2008). Positive control was MMS at 10 or 15 µg/mL (MMS, Merck-Millipore) and negative control was culture medium. For the comet assay, cytotoxicity was assessed at harvest using the Trypan Blue dye exclusion assay. To exclude cytotoxicity as a confounding factor, concentrations which led to more than 70% of cell viability were then submitted to a genotoxicity assessment (Tice et al. 2000).

Cell signaling pathways: Total RNA has been isolated using the miRNeasy Mini Kit (Qiagen). After the reverse transcription of 200 ng of total RNA in single-stranded cDNA using the Superscript™ IV VILO™ Mastermix Kit, the expression profile of 672 target mRNA was carried out using TaqMan® OpenArray® Human Signal Transduction Panel and TaqMan® OpenArray® Real-time MasterMix with a QuantStudio™ 12K Flex Real-Time PCR System equipped with the AccuFill™ robot, and the Relative Quantification application from the ThermoFisher Scientific's cloud (i.e., Fold-Change: FC > 1.5 or < 0.66, p value < 0.05) according to the manufacturer's recommendations (ThermoFisher Scientific). Functional analysis of the differentially regulated gene (DRG) was carried out in silico using Cytoscape v 3.8.2. software (https://cytoscape.org/).

Epigenetic alterations: The Global DNA Methylation LINE-1 Assay provided a measure of global DNA methylation shifts in BEAS-2B cells (Active Motif). Active motif's Histone Purification Mini Kit was used to purify core histones from BEAS-2B cells and ELISA kits were used to determine specific H3 post-translational modifications (i.e., H3K9ac and H3K27ac versus total H3). HAT and HDAC activities of BEAS-2B cells were determined using HAT and HDAC assays from Active motif, according to the manufacturer's recommendations

(Leclercq et al. 2017, Sotty et al. 2019). Moreover, miRNA expression profiles were studied in BEAS-2B cells. Briefly, total RNAs were isolated using the miRNeasy Mini Kit (Qiagen). After the reverse transcription of 100 ng of total RNA in single-stranded cDNA using the TaqMan® MicroRNA Reverse Transcription Kit and the pre-amplification of these cDNA using the TaqMan® PreAmp MasterMix), the expression profile of 754 target miRNA was carried out using Taqman® OpenArray® Human miRNA Panel and TaqMan® OpenArray® Real-time MasterMix with a QuantStudio™ 12K Flex Real-Time PCR System equipped with the AccuFill™ robot, and the Relative Quantification application from the ThermoFisher Scientific's cloud (i.e., Fold-Change: FC > 1.5 or < 0.66, p value < 0.05), according to the manufacturer's recommendations (ThermoFisher Scientific). Functional analysis of the differentially regulated miRNA (DRmiR) was carried out in silico using TargetScanHuman v7.2 (http://www.targetscan.org/vert_72/), miRNA target Prediction Database (miRDB; http://mirdb.org), and et DIANA TOOLS Tarbase V8 (http://carolina.imis.athena-innovation.gr/diana_tools/web/index.php?r=tarbasev8%2Findex).

Apoptotic events: Activities of both some initiator caspases (caspase 8 and caspase 9) and executioner caspases (i.e., caspase 3 and caspase 7) were determined with Caspase Glo® 3/7, Caspase Glo® 8, and Caspase Glo® 9 Assays, as recommended by the manufacturer (Promega). Single-channel dead cell apoptosis kit with Annexin V Pacific Blue™ 488 and SYTOX™ AAdvanced dyes for flow cytometry applications were used as recommended by the manufacturer (ThermoFisher scientific), before BEAS-2B cell analysis using an Attune™ NxT Acoustic Focusing Cytometer (ThermoFisher scientific) to study apoptotic events. Staurosporine (2.5 µM, 24 h)-treated BEAS-2B cells served as a positive control.

Statistical analysis

Results were expressed as mean values and standard deviations. Comparisons were performed between data from exposed BEAS-2B cells (i.e., WF-derived Q-UFP) and those from negative controls. After having checked for the Normal distribution of the variables under study, the Student's t-test ($p < 0.05$) was used to perform statistical analyses (Software: SPSS v27 for windows). For the in vitro comet assay, it has previously been shown that the tail intensity does not follow a Gaussian distribution. Thus, the non-parametric Mann-Whitney U-test was used to evaluate the statistical difference between groups (i.e. between each concentration vs. the respective negative control). All statistical analyses were performed with StatView Software (version 5.0, SAS Institute Inc., SAS Campus Drive, Cary, North Carolina 27513, USA). Differences with a $p<0.05$ were considered statistically significant.

RESULTS

Physical and chemical characteristics of WF-derived Q-UFP

The campaign to produce WF according to GMAW-SS process using an automatic welding bench was realized between the 10th[h] and the 13th of September 2018, with the aim of collecting the Q-UFP ($PM_{0.25}$). The average mass concentration of the total particles was 40.1 ± 3.9 mg/m^3. Fifty-seven welding cords were used to collect 133 mg of Q-UFP. Concentrations in numbers ranged from 6.6 to 11.7x10^6/cm^3 on the entire collection. The Q-UFP represented about 87 % of the total amount of the particles from each generation. The size distribution in number of the WF-derived Q-UFP showed a monomodal distribution centered on a aerodynamic diameter of 104.4 ± 52.3 nm as measured by ELPI+. Analysis of the zeta potential of Q-UFP suspended in MilliQ water (i.e., 1.91 µg/µL) yielded to an average result of -13.8 ± 0.3 mV. As shown in Table 1, total element concentration and total oxide concentration of Q-UFP were 646.9 µg/mg and 944 µg/mg, respectively. Moreover, Q-UFP had high enrichment degrees of certain elements (i.e., Fe > Cr > Mn > Si > Ni) and accordingly certain oxides (i.e., Fe_2O_3 > CrO_3 > MnO > SiO_2 > NiO). Regarding CrVI, the concentration within WF was 160 ± 10 µg/m^3.

Intrinsic oxidative potential of WF-derived Q-PUF

The intrinsic OP of Q-UFP was firstly determined through the CM-H_2DCFDA acellular assay. After the incubation of the CM-H_2DCFDA probe in the continuous presence of Q-UFP at 10, 50 and 100 µg/mL, the relative fluorescence intensities were respectively 7.57, 21.14, and 57.97-fold increased, versus negative control ($p < 0.001$). The relative fluorescence intensity of positive control (i.e., H_2O_2, 100µM) was 27.74-fold increased, versus negative control ($p < 0.001$). Secondly, the intrinsic OP of Q-UFP was determined through glutathione oxidation. There were respectively 14.86, 58.36, and 122.43-fold increases of the GSSG/GSH ratio in presence of Q-UFP at 10, 50 and 100 µg/mL, versus negative control. The positive control lead to a 50.70-fold increase of the ratio.

WF-derived Q-UFP-induced cytotoxicity

The Figures 1-A and 1-B respectively show the intracellular ATP concentrations of BEAS-2B cells after acute or repeated exposures to Q-UFP at concentrations ranging from 0.1 to 50 µg/cm². There were statistically significant dose-dependent decreases of the ATP contents within BEAS-2B cells acutely exposed to Q-UFP at concentrations ≥ 1 µg/cm², or repeatedly exposed to Q-UFP at concentrations ≥ 0.25 µg/cm², versus negative control ($p < 0.05$). Taken together, these results suggested to use the lowly- (i.e., lethal concentration at 10 %, LC_{10}; red dotted lines) and highly (i.e., lethal concentration at 40 %, LC_{40}; black dotted lines)-cytotoxic doses of 1.5 and 9 µg/cm² for the acute scenario of exposure, and the use of the lowly- (i.e., LC_{10}; red dotted lines) and highly (i.e., LC_{40}; black dotted lines)-cytotoxic doses of 0.25 and 1.5 µg/cm² for the repeated scenario of exposure, in order to further investigate the other toxicological endpoints under study.

WF-derived Q-UFP-induced oxidative stress

The Figure 2-A indicates that there was a significant dose-dependent-production of ROS by BEAS-2B cells acutely exposed to Q-UFP at 1.5 or 9 µg/cm², and, to a lesser extent, repeatedly exposed to Q-UFP at 0.25 and 1.5

µg/cm², versus negative control ($p < 0.001$). Moreover, as shown in the Figures 2-B, 2-C, and 2-D, NRF2 signaling pathway was significantly activated in a dose-dependent manner in Q-UFP-exposed BEAS-2B cells, versus negative control. There were also statistically significant increases of NRF2 binding activity in BEAS-2B cells acutely exposed to Q-UFP, only at the highest dose, or repeatedly exposed to Q-UFP, at the two doses ($p < 0.01$). Moreover, the expression of the NRF2-downstream target genes, such as *heme oxygenase-1* (*HMOX*) and *NADPH quinone oxydoreductase 1* (*NQO-1*), was further increased in BEAS-2B cells acutely exposed to Q-UFP at 1.5 or 9 µg/cm², and, to a lesser degree, repeatedly exposed to Q-UFP at 0.25 and 1.5 µg/cm² ($p < 0.05$). Remarkably, for any exposure, despite the early activation of NRF2 signaling pathway, oxidative alterations of glutathione status (i.e., oxidation of GSH into GSSG), DNA (i.e., 8-OHdG), proteins (i.e., carbonylated proteins), and lipids (i.e., 4-HNE) significantly occurred in a dose-dependent manner, versus negative control ($p < 0.05$; Figures 3-A, 3-B, 3-C, and 3-D). However, it is noteworthy that Q-UFP-induced oxidative damage to all these critical macromolecules, except for lipids (i.e., 4-HNE) was generally highest after the acute exposure scenario than after the repeated exposure scenario.

WF-derived Q-UFP-induced cytokine secretion

As shown in Figure 4 A, there were statistically significant increases of the NF-κB binding activity in BEAS-2B cells only after their acute or repeated exposures to the highest dose of Q-UFP, versus negative control ($p < 0.01$). Figures 4-B, 4-D, and 4-F showed the only very slight induction of the gene expression of *TNF-α* in BEAS-2B cells acutely exposed to the highest dose of Q-UFP, and *IL-1β* in BEAS-2B acutely exposed to the two doses of Q-UFP and repeatedly exposed to the highest one ($p < 0.05$). For any exposure, no significant difference of the secretion by BEAS-2B cells of all the inflammatory mediators under study (i.e., RANTES, GM-CSF, GRO-α, IL-1β, IL-6, IL-8, MCP-1, and TNF-α) was reported versus negative control. Figures 4-C, 4-E, and 4-G give some examples for TNF-α, IL-1β, and IL-6.

WF-derived Q-UFP-induced genetic alterations

The *in vitro* comet assay under alkaline conditions was applied to assess primary DNA damage. The cell viability should be more than 70 % to exclude cytotoxicity as a confounding factor. Results of the mean of medians of % DNA in the comet tail and the corresponding relative cell viability obtained in BEAS-2B cells are shown in Figure 5-A, 5-B, and 5-C. For both the standard (i.e., dark grey histogram bars) and the hOGG1-modified (i.e., slight grey histogram bars) comet assays, no increase in DNA damage was observed in acutely exposed BEAS-2B cells (i.e., 4 h or 24 h) or repeatedly exposed BEAS-2B cells (i.e., 3 x 24h) to Q-PUF at doses ranging from 0.25 until 9 µg/cm², versus negative control.

WF-derived-Q-UFP-induced cell signaling pathways

To better decipher the underlying mechanisms triggered by Q-UFP in BEAS-2B cells, DRG known as closely implicated to some cell signaling pathways were investigated. Figures 6-A and 6-B show the down and up- regulated genes, respectively. Indeed, 6 DRG (i.e., 6 down-regulated) were reported in BEAS-2B cells acutely exposed to the lowest dose of Q-UFP, 24 DRG (i.e., 19 down- and 5 up-regulated) in BEAS-2B cells acutely exposed to the highest

dose of Q-UFP, and 39 DRG (i.e., 30 down- and 9 up-regulated) in BEAS-2B cells repeatedly exposed to the highest dose of Q-UFP, versus negative controls. As shown in Figures 6-A and 6-B, only 2 DRG, also down-regulated, (i.e., *Cyclin-dependent kinase 4: CDK4, and Serine/threonine-protein kinase MTOR: MTOR*) were reported as common to all the exposure conditions of BEAS-2B cells to Q-UFP. Moreover, *Heat Shock Protein Family D (Hsp60) Member 1*(*HSPD1*) and *Ras Homolog, MTORC1 Binding* (*REHB*) were the two down-regulated genes common to BEAS-2B cells acutely exposed to the lowest or the highest doses of Q-UFP. Only *REHB* was down-regulated at the same time in BEAS-2B cells acutely exposed to the lowest dose of Q-UFP and in BEAS-2B cells repeatedly exposed to the highest dose of Q-UFP. At least, 6 DRG, 5 down-regulated (i.e., *Janus Kinase 2*: *JAK2*, *Hydroxymethylbilane Synthase*: *HMBS*, *Lymphoid Enhancer Binding Factor*: *1LEF1*, *BCL2 Apoptosis Regulator*: *BCL2*, *Proenkephalin*: *PENK*) and 1 up-regulated (*Pyruvate Dehydrogenase Kinase 1*: *PDK1*) were common to BEAS-2B cells acutely and repeatedly exposed to the highest dose of Q-UFP.

WF-derived Q-UFP-induced epigenetic alterations

Firstly, the Figures 7-A, 7-B, and 7-C show both the HDAC and HAT activities, and their ratio, in BEAS-2B cells, acutely and repeatedly exposed to Q-UFP. In BEAS-2B cells acutely exposed to the highest dose of Q-UFP or repeatedly exposed to the two doses of Q-UFP, there were statistically significant increases of the HDAC activity, versus negative control ($p < 0.01$). Only the repeated scenario of exposure to Q-UFP lead to significant increases of the HAT activity in BEAS-2B cells ($p < 0.001$). Overall, the figure 7-C revealed significant increases of the HDAC activity/HAT activity ratio in BEAS-2B cells repeteadly exposed to the lowest dose of Q-UFP, and acutely or repeatedly exposed to the highest dose of Q-UFP ($p < 0.05$). Moreover, Figures 7-D and 7-E indicated significant decreases of the acetylation of the H3 histone at Lys 9 and Lys 27 in BEAS-2 B cells acutely exposed to the two doses of Q-UFP, but only at Lys 27 in BEAS-2 B cells repeatedly exposed to the two doses of Q-UFP, versus negative control ($p < 0.05$). In addition, no significant modification of the global DNA methylation was observed in BEAS-2B cells for any exposure.

Secondly, to go further in deciphering the underlying mechanisms induced by Q-UFP in BEAS-2B cells, DRmiR were investigated (Figures 8-A and 8-B). Accordingly, 4 DRmiR (i.e., 2 down- and 2-up-regulated) were reported in BEAS-2B cells acutely exposed to the lowest dose of Q-UFP, 7 DRmiR (i.e., 1 down-regulated and 6 up-regulated) in BEAS-2B cells acutely exposed to the highest dose of Q-UFP, 4 DRmiR (i.e., 1 down- and 3 up-regulated) in BEAS-2B cells repeatedly exposed to the lowest dose of Q-UFP, and 5 DRmiR (i.e., 3 down- and 2 up-regulated) in BEAS-2B cells repeatedly exposed to the highest dose of Q-UFP, versus negative controls. As shown in Figures 8-A and 8-B, only 2 DRmiR, also 1 down- and 1-up-regulated (i.e., hsa-miR-551b# and hsa-miR-331-5p, respectively) were reported as common to BEAS-2B cells acutely exposed to the lowest or the highest doses of Q-UFP. Only hsa-miR-210-3p was up-regulated at the same time in BEAS-2B cells acutely exposed to the highest dose of Q-UFP and in BEAS-2B cells repeatedly exposed to the lowest dose of Q-UFP.

Thirdly, functional analysis of the up-regulated DRmiR founded in BEAS-2B acutely or repeatedly exposed to Q-PUF was carried out in silico using three complementary miRNA target Prediction Database (i.e., TargetScanHuman v7.2, miRDB, and DIANA TOOLS Tarbase V8), and thereafter compared with the DRG previously identified. Figures 9-A to 9-J showed the results as Venn Diagrams of hsa-miR-331-5p, hsa-miR-210-3p,

hsa-miR-424-5p, hsa-miR-597-5p, hsa-miR-212-3p, hsa-miR-1260a, hsa-miR-1248, hsa-miR-625-5p, hsa-miR-744-3p, and hsa-miR-766-3p, respectively. Indeed, 19 target genes, only predicted by TargetScanHuman v7.2, were founded within the DRG reported in BEAS-2B cells acutely and/or repeatedly exposed to Q-UFP: *Apoptosis Regulator: BCL2, Janus kinase 2: JAK2, SMAD Family Member 4: SMAD4, Cyclin-dependent kinase 4: CDK4, Inhibitor Of Nuclear Factor Kappa B Kinase Regulatory Subunit Gamma: IKBKG, RAS P21 Protein Activator 1: RASA1, caspase 1: CASP1, MYD88 Innate Immune Signal Transduction Adaptor:MYD88, Mitogen-Activated Protein Kinase Kinase Kinase 7: MAP3K7, Transcription Factor 7: TCF7, Cyclin B1: CCNB1, Signal Transducer And Activator Of Transcription 5A: STAT5A, Myocyte Enhancer Factor 2C: MEF2C, Lysophosphatidic Acid Receptor 2: LPAR2, Toll Like Receptor 4T: LR4, Toll Like Receptor 6T LR6, NKD Inhibitor Of WNT Signaling Pathway 1: NKD1, Solute Carrier Family 44 Member 2: SLC44A2, and Calcitonin Receptor Like Receptor: CALCRL. Galanin Receptor 2 (GALR2)* was the target gene only predicted by miRDB, also reported within the DRG reported in BEAS-2B cells acutely and/or repeatedly exposed to Q-UFP. Moreover, 10 target genes, only predicted by DIANA TOOLS Tarbase V8, were among the DRG of BEAS-2B cells acutely and/or repeatedly exposed to Q-UFP: *SMAD Family Member 4: SMAD4, Peroxisome Proliferator Activated Receptor Gamma: PPARG, NKD Inhibitor Of WNT Signaling Pathway 1: NKD1, Apoptosis Regulator: BCL2, Cyclin-dependent kinase 4: CDK4, Toll Like Receptor 6T LR6, Lymphoid Enhancer Binding Factor 1: LEF1, Lysophosphatidic Acid Receptor 2: LPAR2, Adenosine A1 Receptor: ADORA1, and Calcitonin Receptor Like Receptor: CALCRL.* Some target genes also founded among the DRG of BEAS-2B cells acutely and/or repeatedly exposed to Q-UFP were predicted by two of the three miRNA target Prediction Databases: *Transcription Factor 7: TCF7, Proenkephalin: PENK, Apoptosis Regulator: BCL2, Lymphoid Enhancer Binding Factor 1: LEF1, Wnt Family Member 5B: WNT5B* by TargetScanHuman v7.2 and miRDB, on the one hand, and *Inhibitor Of Nuclear Factor Kappa B Kinase Regulatory Subunit Gamma: IKBKG and Kinase Suppressor Of Ras: KSR1* by TargetScanHuman v7.2 and DIANA TOOLS Tarbase V8, on the other hand. At least, only three target genes also founded within the DRG of BEAS-2B cells acutely and/or repeatedly exposed to Q-UFP were predicted by all the three miRNA target Prediction Databases: Neural Cell Adhesion Molecule 1: *NCAM1, RAS P21 Protein Activator 1: RASA1, Adenosine A1 Receptor: ADORA1.*

WF-derived Q-UFP-induced apoptotic events

Figure 10-A revealed significant increases of the Annexin V labelling for any exposure scenario of BEAS-2B cells to Q-PUF ($p \leq 0.05$). Moreover, acute and repeated exposure of BEAS-2B cells to the highest doses of Q-UFP significantly activate initiator caspase-8, initiator caspase-9, and effector caspase-3/7, versus negative controls ($p \leq 0.01$, Figures 10-B, 10-C, and 10-D).

DISCUSSION

Although the current literature supported that the combustion-derived PM emitted within WF will represent the driving force of this occupational hazard, researchers are still far from having a fully detailed mechanistic explanation for its respiratory toxicity. Using a human bronchial epithelial cell model, we also try to better decipher the cellular and molecular underlying mechanisms of toxicity triggered by the WF-derived Q-UFP fraction.

Firstly, WF were produced according to GMAW-SS process with an automatic welding bench and Q-UFP were collected based on their aerodynamic diameter. The nanometric monomodal size distribution by number of these WF-derived Q-UFP was centered on 104.4 ± 52.3 nm, in keeping with the size characteristics published by Kirichenko et al. (2018). Antonini et al. (2017), studying the size distribution of all the particles within WF, indicated a multi-modal distribution because of the agglomeration, chain-like structures, of the majority of the nanometer-size primary particles collected in the submicron size range, and only a very small amount (< 5%) of non-agglomerated UFP. The metal composition of the WF-derived Q-UFP under study revealed high concentrations of certain elements (i.e., Fe > Cr > Mn > Si > Ni) and, accordingly, oxides (i.e., Fe_2O_3 > Cr_2O_3 > MnO > SiO_2 > NiO), as published by Antonini et al. (2017), Badding et al. (2014), Falcone et al. (2018a,2018b), Leonard et al. (2010), and McCarrick et al. (2019). According to McCarrick et al. (2019), because of the use of SS, high concentrations of CrVI (i.e., 160 ± 10 µg/m^3) were found, representing 3% of the total mass of Cr. Taken together, the physical and chemical characteristics of the WF-derived Q-UFP emitted by GMAW-SS were close to those generally encountered in occupational settings, proving once again that welding operations are procedures with high levels of Q-UFP hazard for human health.

Thereafter, in order to contribute to the better knowledge of the cellular and molecular underlying mechanisms by which WF-derived Q-UFP exerts their toxicity, BEAS-2B cells were acutely or repeatedly exposed to such Q-UFP at relatively low doses (i.e., 1.5 and 9 µg/cm², and 0.25 and 1.5 µg/cm², respectively). The doses we applied were among the lowest reported to give harmful effects whilst limiting a massive cell death (Boublil et al. 2013; Gualtieri et al. 2018; Leclercq et al. 2016, 2017, 2018; Longhin et al. 2019; Platel et al; 2019; Sotty et al. 2019, 2020). Indeed, ATP concentrations within BEAS-2B cells acutely or repeatedly exposed to Q-UFP supported both the use of a low (i.e., DL_{10}) and a moderate (i.e., DL_{40}) doses, thereby allowing to keep sufficient effective doses to study these underlying mechanisms while contributing to the effort to be as closer as possible to the human exposure levels at the workplaces.

Oxidative stress is one of the underlying mechanisms generally involved in air pollutant-induced adverse health effects (Abbas et al. 2010, 2013, 2016, 2019; Badran et al. 2020; Bocchi et al. 2016; Garçon et al. 2006; Gualtieri et al. 2010, 2011; Leclercq et al. 2016, 2017a, 2018; Longhin et al. 2013, 2016, Sotty et al. 2019, 2020). Firstly, the intrinsic OP of Q-UFP was reported through the dose-dependent oxidation of both CM-H_2DCFDA and glutathione in acellular assays. Of course, this result must be related to the metal (e.g., Fe > Cr > Mn > Si > Ni) and oxide (e.g., Fe_2O_3 > Cr_2O_3 > MnO > SiO_2 > NiO) composition of the Q-UFP under study. Badding et al. (2014) indicated that Fe makes up the majority of GMAW-SS metals, and that transition metals such as Fe and Cr, in addition to Mn, Ni, and Cu (i.e., 259.8, 129.4, 127.6, 43.2, and 4 ng/µg, respectively, in the Q-UFP we studied) participate in Fenton reduction/oxidation cycling and are known to mediate ROS production. Ghanem et al. (2021) recently reported that

transition metals in the both the SS-derived WF and MS-derived WF, mainly composed of Fe, Mn, Zn, Cu, Cr, and Ni in various proportions, have shown different solubility and also different contributions to their intrinsic OP, Mn (II), Cu (II), and Ni (II) being the most active. Garçon et al. (2001) showed the important role of iron oxides (i.e., Fe_2O_3 and Fe_3O_4) in the over-production of ROS in several cell and animal models. Leonard et al. (2010) demonstrated that WF were able to induce ROS over-production over a range of particle sizes, the smaller particle size (i.e., 0.032-0.180 μm) showing the most reactivity and the greater ROS potential, and that WF-derived PM emitted by GMAW-SS showed a higher reactivity and ROS capacity. Taken together, all these results supported the crucial role played by the chemical composition of SS on the ROS generation capacity thanks to the presence of Cr and Ni, and other transition metals, such as Fe, Mn, and Cu. Secondly, after having shown the intrinsic OP of Q-UFP, we sought to evaluate their ability to effectively produce massive oxidative damage in a relevant cell model. Accordingly, we demonstrated that Q-UFP highly oxidized all the cellular macromolecules in a dose-dependent manner in BEAS-2B cells acutely or repeatedly exposed. As a consequence, there was a dose-dependent activation of the specific antioxidant NRF2 signaling pathway, as assessed by the NRF2 binding activity and the expression of *HMOX* and *NQO-1*, two of the NRF2-downstream target genes, in BEAS-2B cells acutely and, to a lesser extent, repeatedly exposed to Q-UFP. Because of its key role as master regulator of the cell redox homeostasis, NRF-2 is also well-equipped to counteract ROS production and is critical for maintaining the redox balance in the cell (Wardyn et al. 2015). Leclercq et al. (2018) and Sotty et al. (2020), studying the NRF2 signaling pathway activation within BEAS-2B cells repeatedly exposed to fine or ultrafine particles supported the key role played by this transcriptional factor to counteract ROS over-production. However, despite the early activation of NRF2 signaling pathway, there were massive oxidative alterations of the cellular constituents, such as DNA, proteins, and/or lipids, in BEAS-2B cells after any exposure to WF-derived Q-PUF. Hence, in this work, because of the inability of the NRF2 signaling pathway to totally ward off ROS over-production, the antioxidant defenses-induced by NRF2 were exceeded in BEAS-2B cells acutely and/or repeatedly exposed. Oxidative damage to DNA, proteins and/or lipids can also disrupt the cell homeostasis, thereby contributing to gene expression deregulation, DNA mutation, protein alteration with loss of function, and lipid peroxidation with loss of membrane integrity and/or fluidity (Abbas et al. 2019; Badran et al. 2020; Garçon et al., 2006; Gualtieri et al. 2010, 2011; Leclercq et al. 2016, 2017a, 2018; Longhin et al. 2013, 2016; Sotty et al. 2020). Accordingly, Grazyk et al. (2016), indicated that, 3 h after the short-term exposure to GMAW-SS WF, even in controlled and well-ventilated settings, there were acute oxidative stress reactions in healthy, non-smoking individuals not chronically exposed to WF, as shown by significant increases in plasma and urinary-H_2O_2 concentrations, and plasma and urinary-8-OHdG concentrations.

In order to maintain essential coordinated cellular responses needed to resolve the unbalanced status of the cells and/or tissues, NRF2 and NF-κB cell signaling pathways, that respectively regulate cellular responses to oxidative stress and inflammation, must closely interplay through multiple molecular interactions, which can often depend on the cell types and tissue contexts (Wardyn et al. 2015). However, in this work, despite the significant increase of the anti-inflammatory NRF2 binding to ARE, there was a significant activation of the pro-inflammatory NF-κB cell signaling pathway in BEAS-2B cells repeatedly exposed to Q-UFP at their highest dose. Nevertheless, only a very slight induction of the gene expression of *TNF-α* and *IL-1β* in BEAS-2B cells acutely and repeatedly exposed to the

highest dose of Q-UFP was reported, without any significant secretion of their proteins, or those of other pro-inflammatory mediators (i.e., RANTES, GM-CSF, GRO-α, IL-6, IL-8, and MCP-1). Despite our efforts to quantify the protein expression of these inflammatory mediators in the cell-free supernatants of BEAS-2B cells using different methods (i.e., Luminex and MSD assays), we failed to obtain consistent results in the BEAS-2B cells exposed to WF-derived Q-UFP. Interestingly, other authors, having already encountered the same difficulties, have incriminated some artefactual interactions of UFP with these inflammatory mediators, thereby creating non-biological artifacts when measuring their concentrations in biological matrices (Brown et al. 2010; Saleh et al. 2019; Veranth et al. 2007). Accordingly, Badding et al. (2014), testing the hypothesis that some pro-inflammatory mediators may be produced by unprimed RAW 264.7 cells 24 h after their exposure to GMAW-SS-derived WF, reported some non-significant increases (i.e., *TNF-*α and IL-6), thereby supporting the general statement that WF are not able to robustly produce pro-inflammatory mediators from various cell models, including unprimed macrophages. In contrast, other authors evaluating the pro-inflammatory potent of WF-derived particles through animal experiments, observed transient but significant elevated markers of lung inflammation, as shown by total cells and/or neutrophils in bronchioalveolar lavage fluid and cytokine and/or chemokine secretion (Antonini et al. 2017; Ederly et al. 2011; Falcone et al. 2018a). Moreover, Krishnaraj et al. (2017a, 2017b), investigating the effect of WF in rats, reported increased levels ROS in lung tissues associated with accumulation of 8-OHdG and, at the same time, activation of both NRF2 and NFκB signaling pathways, thereby leading to the significant secretion of pro-inflammatory mediators. In addition, Jarvela et al. (2012) investigating occupational exposure to WF generated from grinding MS plates or pieces in current workplaces, reported a slight acute inflammation in metal workers by means of alterations of the total blood leukocytes and neutrophils, as well as IL-1β and E-selectin, but no changes of the pulmonary function, after the work shift.

Because oxidative DNA damage, such as 8-OHdG, occurs not only in cell models but also in humans exposed to WF, we next sought to elucidate whether WF-derived Q-UFP contribute to other genetic alterations. However, under our experimental conditions, there was no significant primary DNA damage, as evaluated using the *in vitro* standard comet assay under alkaline conditions and the hOGG1-modified version. Other authors, reported the ability of GMAW-MS and, to a higher extent, GMAW-SS-derived WF to produce DNA double-strand breaks, and incriminated the high levels of CrVI, Ni and/or Mn (Badding et al. 2014; Leonard et al. 2010; McCarrick et al. 2019). Accordingly, Antonini et al. (2005) showed that CrVI within WF emitted by MMA-SS induced DNA damage, that was similar to what they observed when using a soluble Cr salt, likely as a result from hydroxyl radical formation. However, here, the doses of Q-UFP we applied on the BEAS-2B cell model seemed to be too low to produce any significant primary DNA damage.

Thereafter, to go further in better deciphering the molecular mechanisms underlying the toxicity of WF-derived Q-UFP, some critical DRG involved in the activation of some key cell signaling pathways were identified in BEAS-2B cells acutely and repeatedly exposed. Accordingly, 6 DRG (i.e., 6 down-regulated) were reported in BEAS-2B cells acutely exposed to the lowest dose of Q-UFP, and 24 DRG (i.e., 19 down- and 5 up-regulated) in BEAS-2B cells acutely exposed to the highest dose of Q-UFP, whereas 39 DRG (i.e., 30 down- and 9 up-regulated) were found in BEAS-2B cells repeatedly exposed to the highest dose of Q-UFP, thereby supporting the highest effects of this

later. Interestingly, 2 DRG (i.e., *Cyclin-dependent kinase 4: CDK4, and Serine/threonine-protein kinase MTOR: MTOR*), generally described as closely involved in cell cycle regulation, were reported as down-deregulated for any exposure (Guo et al. 2021). Moreover, the 6 DRG, 5 down-regulated (i.e., *Janus Kinase 2*: *JAK2*, *Hydroxymethylbilane Synthase*: *HMBS*, *Lymphoid Enhancer Binding Factor*: *1LEF1*, *BCL2 Apoptosis Regulator*: *BCL2*, *Proenkephalin*: *PENK*) and 1 up-regulated (*Pyruvate Dehydrogenase Kinase 1*: *PDK1*), common to BEAS-2B cells acutely and repeatedly exposed to the highest dose of Q-PUF, supported the alteration of some key regulators of cell cycle, generally members of anti-apoptotic signaling pathways (Tandawy et al. 2020, Yildirim et al. 2021, Tungsukruthai et al. 2021). Zeilder-Ederly et al. (2010), in their comprehensive transcriptional profiling, also revealed differences in the DRG and gene networks triggered by WF according to mouse strains: gene expression was more deregulated in the susceptible A/J strain, and exposure to WF-emitted by GMAW-SS was associated with overexpression of immunomodulatory genes. Erdely et al. (2011) reported some DRG closely involved in inflammation (*e.g.*, *TNF-*α, *IL1-*β), stress (e.g., *HMOX, NQO1*), coagulation, adhesion, and remodeling/growth factors in mice exposed to WF, but with some difference according to their emission by MMA-SS, GMAW-SS, and GMAW-MS. Moreover, Falcone et al. (2018a), exposing mice to WF emitted by GMAW-SS supported the above-mentioned results and the differential inflammatory and/or stress responses elicited depending on the type of WF. Oh et al. (2011), exposing rats to WF emitted by MMA-SS, also reported DRG profiles related to inflammation and repair processes, rapidly, dynamically, and stringently regulated in many biological diseases and pathological processes. At least, exposure to WF emitted by GMAW-SS induced 37 DRG coding for DNA damage sensors, cell cycle arrest in G1/S phase, DNA repair enzymes, and caspase-mediated apoptosis within rat lungs (Krishnaraj et al. 2017a, 2017b).

Moreover; recent evidence supported that critical alterations of the epigenome can occur after exposure to air pollution-derived PM and thereafter lead to severe dysregulation of gene expression within the lung (Leclercq et al. 2017a; Sotty et al. 2019). Therefore, a better knowledge of these epigenetic changes may provide an additional tool for analyzing the association between WF-derived Q-UFP exposure and the development and/or exacerbation of chronic inflammatory lung diseases, including cancers. However, here, no significant change of the global DNA methylation was observed in BEAS-2B cells after any exposure to Q-PUF. Shoeb et al. (2017), trying to identify potential biomarkers of epigenetic changes in isolated peripheral blood mononuclear cells of animal models after their exposure to WF, including GMAW-MS and MMA-SS, reporting similar results. With regards to histone H3 PTM, the significant deacetylation of the H3 histone at Lys 9 and Lys 27 in BEAS-2 B cells acutely exposed to the two doses of Q-PUF, but only at Lys 27 in BEAS-2 B cells repeatedly exposed to the two doses of Q-PUF, were consistent with the related enzyme. However, to our current knowledge, only very few data are available about histone H3 PTM by WF. Histone acetylation/deacetylation could be closely related to the development or exacerbation of chronic inflammatory lung diseases, and even cancers (Li et al. 2015).

While miRNA are now well-known regulators in almost all cellular signaling pathways and can target up to several hundred mRNA, studying the aberrant miRNA expression and their predicted interactions with the ahead-identified DRG. appeared to be highly relevant (Acunzo et al. 2015). For any exposure, the number of DRmiR reported in BEAS-2B remained relatively weak, ranging from 4 to 7. Among them, only 2 DRmiR, also 1 down- and

1 up-regulated (i.e., has-miR-551b# and has-miR-331-5p, respectively) were reported as common to BEAS-2B cells acutely exposed to the lowest or the highest doses of Q-UFP, and only one (i.e., has-miR-210-3p) was up-regulated at the same time in BEAS-2B cells acutely exposed to the highest dose of Q-UFP and repeatedly exposed to the lowest dose of Q-UFP. Xu et al. (2014) founds that miR-551b# up-regulation in apoptotic-resistant cells inhibited the expression of antioxidant enzymes, and potentiated ROS accumulation and mucin expression. While no information is currently available about the role of has-miR-331-5p in lung cells, Ren et al. (2019), studying and comparing the expression of miR-210-3p in different non-small cell lung cancer cell (NSCLC) lines and BEAS-2B cell line, indicated that it can regulate the proliferation and apoptosis by targeting *Transcription Regulator Family Member A*. However, as highlighted by Jardim et al. (2011) and Vrijens et al. (2105), although miRNA changes may be sensitive indicators of the effects of acute and chronic environmental exposure such as WF-derived Q-UFP, further studies should be conducted to elucidate the role of the mediation effect of miRNA between the exposure and the effect to provide a more accurate evaluation of the consequences of these miRNA changes.

The functional analysis of the up-regulated DRmiR founded in BEAS-2B acutely or repeatedly exposed to Q-PUF, carried out in silico using three complementary miRNA target Prediction Database (i.e., TargetScanHuman v7.2, miRDB, and DIANA TOOLS Tarbase V8), and compared to the above-mentioned DRG, supported the deregulation of some relevant cellular signaling pathways closely involved in cell inflammation (e.g., *IKBKG*, *NCAM1*, *MYD88, TCF7, TLR4, TLR6, LPAR2,* and *CALCRL),* and, to a higher extent, cell cycle deregulation (e.g., *BCL2, JAK2, SMAD4, RASA1, CASP1, CCND1, ADORA1, STAT5, KSR1, MEF2C, NKD1,* and WNT5B). Some of the identified DRmiR and target DRG being closely implicated in the regulation of cell cycle and, in particular, in the fate of the cell to enter into apoptosis, some key events of this regulated cell death were thereafter investigated. Annexin V labelling together with initiator caspase-8, initiator caspase-9, and effector caspase 3/7 activation within BEAS-2B cells whatever their exposure to Q-PUF revealed some apoptotic cells. Accordingly, after 12 weeks of exposure to WF emitted by GMAW-SS, Krishnaraj et al. (2017a, 2017b) reported that the earlier triggered DNA domain repair (DDR) was also compromised as reflected by resumption of the cell cycle, repair inhibition, and failure of apoptosis. Their data clearly supported that exposure to WF influences two crucial layers of inclusive DDR regulation, phosphorylation of key proteins in nonhomologous end-joining (NHEJ), homologous recombination (HR), as well as the ncRNAs that epigenetically modulate DDR, thereby highlighting the concomitant occurrence of severe DNA damage coupled with non-productive DNA repair and apoptosis avoidance, which could contribute to neoplastic transformation. Moreover, Antonini et al. (2005) using an animal model, observed a time-dependent increase in the number of apoptotic cells in the lung airspaces and parenchyma of animals intratracheally instilled with the MMA-SS welding sample.

Overall, the present original results clearly demonstrated for the first time, in a relevant human bronchial epithelial cell model, the crucial role played by the specific metal enriched Q-UFP fraction of the WF emitted by GMAW-SS in ROS over-production, thereby triggering massive oxidative damage, genetic and/or epigenetic alteration, and, therefore, some critical cellular signaling pathways related to oxidative stress, inflammation, and cell cycle deregulation in favor of apoptosis cell death. Future works are still needed to go further in the better knowledge of the respective toxicity potentials of the different metals (e.g., Fe, Cr, Mn, Ni, Cu) within WF-derived Q-UFP. Nonetheless, all these new findings underlined the urgent need to include the Q-UFP fraction of WF in current air

710 quality standards and/or guidelines relevant to the occupational settings, because Q-UFP were certainly shown as
711 participating for a very large part of the human health effects induced by WF.
712

FUNDING SOURCES

This work benefited from grants or contributions from “Association de Santé au Travail 59-62”, “Institut National de Recherche et de Sécurité”, “Institut Mines Telecom Lille Douai”, University of Lille, and the CLIMIBIO and CaPPA projects. The CaPPA project (Chemical and Physical Properties of the Atmosphere) is funded by the French National Research Agency (ANR) through the PIA (Programme d'Investissement d'Avenir) under contract “ANR-11-LABX-0005-01” and by the Regional Council “Hauts-de-France”, and the “European Funds for Regional Economic Development” (FEDER).

CONFLICT OF INTEREST

All authors of this manuscript do not have any financial and personal relationships with other people or organizations that could inappropriately influence their work.

REFERENCES

Abbas I, Garçon G, Saint-Georges F, André V, Gosset P, Billet S, Le Goff J, Verdin A, Mulliez P, Sichel F, Shirali P. Polycyclic aromatic hydrocarbons within airborne particulate matter (PM2,5) produced DNA bulky stable adducts in a human lung cell coculture model. J Appl Toxicol. 2013 33: 109-119.

Abbas I, Verdin A, Escande F, Saint-Georges F, Cazier F, Mulliez P, Courcot D, Shirali P, Gosset P, Garçon G. In vitro short-term exposure to air pollution $PM_{2.5-0.3}$ induced cell cycle alterations and genetic instability in a human lung cell coculture model. Env Res. 2016 147: 146-158.

Abbas I., Badran G., Verdin A., Ledoux F., Roumié M., Courcot D., Garçon G. Polycyclic aromatic hydrocarbon derivatives in airborne particulate matter: sources, analysis and toxicity. Environ. Chem. Lett. 2018 16: 439–475.

Abbas I, Badran G, Verdin A, Ledoux F, Roumie M, Lo Guidice JM, Courcot D, Garçon G. In vitro evaluation of organic extractable matter from ambient $PM_{2.5}$using human bronchial epithelial BEAS-2B cells: Cytotoxicity, oxidative stress, pro-inflammatory response, genotoxicity, and cell cycle deregulation. Environ Res. 2019 171: 510-522.

Acunzo M, Romano G, Wernicke D, Croce CM. MicroRNA and cancer--a brief overview. Adv Biol Regul. 2015 57:1-9.

Anthérieu S, Garat A, Beauval N, Soyez M, Allorge D, Garçon G, Lo-Guidice JM. Comparison of cellular and transcriptomic effects between electronic cigarette vapor and cigarette smoke in human bronchial epithelial cells. Toxicol In Vitro. 2017 45(Pt 3): 417-425.

Antonini JM, Lawryk NJ, Murthy GG, Brain JD. Effect of welding fume solubility on lung macrophage viability and function in vitro. J Toxicol Environ Health A. 1999 58(6): 343-63.

Antonini JM, Leonard SS, Roberts JR, Solano-Lopez C, Young SH, Shi X, Taylor MD. Effect of stainless steel manual metal arc welding fume on free radical production, DNA damage, and apoptosis induction. Mol Cell Biochem. 2005 279(1-2):17-23.

Antonini JM, Stone S, Roberts JR, Chen B, Schwegler-Berry D, Afshari AA, Frazer DG. Effect of short-term stainless steel welding fume inhalation exposure on lung inflammation, injury, and defense responses in rats. Toxicol Appl Pharmacol. 2007 223(3): 234-45.

Antonini JM, Roberts JR, Stone S, Chen BT, Schwegler-Berry D, Frazer DG. Short-term inhalation exposure to mild steel welding fume had no effect on lung inflammation and injury but did alter defense responses to bacteria in rats. Inhal Toxicol. 2009 21(3): 182-92.

Antonini JM, Badding MA, Meighan TG, Keane M, Leonard SS, Roberts JR. Evaluation of the pulmonary toxicity of a fume generated from a nickel-, copper-based electrode to be used as a substitute in stainless steel welding. Environ Health Insights. 2014 8(Suppl 1): 11-20.

Antonini JM, Afshari A, Meighan TG, McKinney W, Jackson M, Schwegler-Berry D, Burns DA, LeBouf RF, Chen BT, Shoeb M, Zeidler-Erdely PC. Aerosol characterization and pulmonary responses in rats after short-term inhalation of fumes generated during resistance spot welding of galvanized steel. Toxicol Rep. 2017. 4: 123-133.

765 Badding MA, Fix NR, Antonini JM, Leonard SS. A comparison of cytotoxicity and oxidative stress from welding
766 fumes generated with a new nickel-, copper-based consumable versus mild and stainless steel-based welding in
767 RAW 264.7 mouse macrophages. PLoS One. 2014 30;9(6): e101310.
768 Badran G, Ledoux F, Verdin A, Abbas I, Roumie M, Genevray P, Landkocz Y, Lo Guidice JM, Garçon G, Courcot
769 D. Toxicity of fine and quasi-ultrafine particles: Focus on the effects of organic extractable and non-extractable
770 matter fractions. Chemosphere. 2020a 243: 125440.
771 Badran G, Verdin A, Grare C, Abbas I, Achour D, Ledoux F, Roumie M, Cazier F, Courcot D, Lo Guidice JM,
772 Garçon G. Toxicological appraisal of the chemical fractions of ambient fine ($PM_{2.5-0.3}$) and quasi-ultrafine
773 ($PM_{0.3}$) particles in human bronchial epithelial BEAS-2B cells. Environ Pollut. 2020b 263(Pt A): 114620.
774 Bocchi C, Bazzini C, Fontana F, Pinto G, Martino A, Cassoni F. Characterization of urban aerosol: seasonal
775 variation of mutagenicity and genotoxicity of $PM_{2.5}$, PM1 and semi-volatile organic compounds. Mutat. Res.
776 Genet. Toxicol. Environ. Mutagen. 2016 807: 16-23.
777 Bonthoux F. Factors Affecting the Capture Efficiency of a Fume Extraction Torch for Gas Metal Arc Welding.
778 Ann Occup Hyg. 2016 Jul;60(6):761-70.
779 Boublil L, Assémat E, Borot MC, Boland S, Martinon L, Sciare J, Baeza-Squiban A. Development of a repeated
780 exposure protocol of human bronchial epithelium *in vitro* to study the long-term effects of atmospheric
781 particles. Toxicol in vitro 2013 27: 533-542.
782 Brown DM, Dickson C, Duncan P, Al-Attili F, Stone V. Interaction between nanoparticles and cytokine proteins:
783 impact on protein and particle functionality. Nanotechnology. 2010 21(21):215104.
784 Burlinson B., Tice R.R., Speit G., Agurell E., Brendler-Schwaab S.Y., Collins A.R., Escobar P., Honma M.,
785 Kumaravel T.S., Nakajima M., Sasaki Y.F., Thybaud V., Uno Y., Vasquez M., Hartmann A. Fourth
786 International Workgroup on Genotoxicity testing: Results of the in vivo Comet assay workgroup. Mutation
787 Research/Genetic Toxicology and Environmental Mutagenesis 2007 627: 31–35.
788 Cazier F, Genevray P, Dewaele D, Nouali H, Verdin A, Ledoux F, Hachimi A, Courcot L, Billet S, Bouhsina S,
789 Shirali P, Garçon G, Courcot D. Characterisation and seasonal variations of particles in the atmosphere of rural,
790 urban and industrial areas: Organic compounds. J Environ Sci (China). 2016 44: 45-56.
791 Chang C, Demokritou P, Shafer M, Christiani D. Physicochemical and toxicological characteristics of welding
792 fume derived particles generated from real time welding processes. Environ Sci Process Impacts. 2013 15(1):
793 214-24.
794 Collins AR, Duthie SJ, Dobson VL. Direct enzymic detection of endogenous oxidative base damage in human
795 lymphocyte DNA. Carcinogenesis. 1993; 14(9): 1733-5. PMID: 8403192.
796 Crobeddu B, Baudrimont I, Deweirdt J, Sciare J, Badel A, Camproux AC, Bui LC, Baeza-Squiban A. Lung
797 Antioxidant Depletion: A Predictive Indicator of Cellular Stress Induced by Ambient Fine Particles. Environ
798 Sci Technol. 2020 54(4): 2360-2369.
799 Devos D, Moreau C, Kyheng M, Garçon G, Rolland AS, Blasco H, Gelé P, Timothée Lenglet T, Veyrat-Durebex
800 C, Corcia P, Dutheil M, Bede P, Jeromin A, Oeckl P, Otto M, Meininger V, Danel-Brunaud V, Devedjian JC,
801 Duce JA, Pradat PF. A ferroptosis-based panel of prognostic biomarkers for Amyotrophic Lateral Sclerosis. Sci
802 Rep. 2019 10(1): 3312.

Erdely A, Salmen-Muniz R, Liston A, Hulderman T, Zeidler-Erdely PC, Antonini JM, Simeonova PP. Relationship between pulmonary and systemic markers of exposure to multiple types of welding particulate matter. Toxicology. 2011 287(1-3):153-9.

Falcone LM, Erdely A, Meighan TG, Battelli LA, Salmen R, McKinney W, Stone S, Cumpston A, Cumpston J, Andrews RN, Kashon M, Antonini JM, Zeidler-Erdely PC. Inhalation of gas metal arc-stainless steel welding fume promotes lung tumorigenesis in A/J mice. Arch Toxicol. 2017 91(8): 2953-2962.

Falcone LM, Erdely A, Salmen R, Keane M, Battelli L, Kodali V, Bowers L, Stefaniak AB, Kashon ML, Antonini JM, Zeidler-Erdely PC. Pulmonary toxicity and lung tumorigenic potential of surrogate metal oxides in gas metal arc welding-stainless steel fume: Iron as a primary mediator versus chromium and nickel. PLoS One. 2018 13(12): e0209413.

Garçon G, Shirali P, Garry S, Fontaine M, Zerimech F, Martin A, Hannothiaux MH. Polycyclic aromatic hydrocarbon coated onto Fe_2O_3 particles: assessment of cellular membrane damage and antioxidant system disruption in human epithelial lung cells (L132) in culture. Toxicol Lett. 2000 117(1-2):25-35.

Garçon G, Zerimech F, Hannothiaux M, Gosset P, Martin A, Marez T, Shirali P. Antioxidant defense disruption by polycyclic aromatic hydrocarbons-coated onto Fe_2O_3 particles in human lung cells (A549). Toxicology. 2001 166(3): 129-37.

Garçon G, Dagher Z, Zerimech F, Ledoux F, Courcot D, Aboukais A, Puskaric E, Shirali P (2006) Dunkerque city air pollution particulate matter-induced cytotoxicity, oxidative stress and inflammation in human epithelial lung cells (L132) in culture. Toxicol in vitro 20: 519-528.

Ghanem M, Perdrix E, Alleman L.Y., Rousset D., Coddeville P. Phosphate Buffer Solubility and Oxidative Potential of Single Metals or Multielement Particles of Welding Fumes. Atmosphere. 2021 12: 30.

Gliga AR, Taj T, Hedmer M, Assarsson E, Rylander L, Albin M, Broberg K. Mild steel welding is associated with alterations in circulating levels of cancer-related proteins. Arch Toxicol. 2019 93(12): 3535-3547.

Grigg J, Miyashita L, Suri R. Pneumococcal infection of respiratory cells exposed to welding fumes; Role of oxidative stress and HIF-1 alpha. PLoS One. 2017 12(3): e0173569.

Gualtieri M, Øvrevik J, Holme JA, Perrone MG, Bolzacchini E, Schwarze PE, Camatini M Differences in cytotoxicity versus pro-inflammatory potency of different PM fractions in human epithelial lung cells. Toxicol In Vitro 2010 24: 29-39.

Gualtieri M, Ovrevik J, Mollerup S, Asare N, Longhin E, Dahlman HJ, Camatini M, Holme JA Airborne urban particles (Milan winter-$PM_{2.5}$) cause mitotic arrest and cell death: Effects on DNA mitochondria AhR binding and spindle organization. Mutat Res. 2011 713: 18-31.

Gualtieri M, Grollino MG, Consales C, Costabile F, Manigrasso M, Avino P, Aufderheide M, Cordelli E, Di Liberto L, Petralia E, Raschellà G, Stracquadanio M, Wiedensohler A, Pacchierotti F, Zanini G. Is it the time to study air pollution effects under environmental conditions? A case study to support the shift of in vitro toxicology from the bench to the field. Chemosphere. 2018 207: 552-564.

Guha N, Loomis D, Guyton KZ, Grosse Y, El Ghissassi F, Bouvard V, Benbrahim-Tallaa L, Vilahur N, Muller K, Straif K; International Agency for Research on Cancer Monograph Working Group. Carcinogenicity of welding, molybdenum trioxide, and indium tin oxide. Lancet Oncol. 2017 18(5): 581-582.

841 Guo M, Liu Z, Si J, Zhang J, Zhao J, Guo Z, Xie Y, Zhang H, Gan L. Cediranib Induces Apoptosis, G1 Phase Cell
842 Cycle Arrest, and Autophagy in Non-Small-Cell Lung Cancer Cell A549 In Vitro. Biomed Res Int. 2021 2021:
843 5582648.
844 Järvelä M, Kauppi P, Tuomi T, Luukkonen R, Lindholm H, Nieminen R, Moilanen E, Hannu T. Inflammatory
845 response to acute exposure to welding fumes during the working day. Int J Occup Med Environ Health. 2013
846 26(2):220-9.
847 Kirichenko KY, Agoshkov AI, Drozd VA, Gridasov AV, Kholodov AS, Kobylyakov SP, Kosyanov DY,
848 Zakharenko AM, Karabtsov AA, Shimanskii SR, Stratidakis AK, Mezhuev YO, Tsatsakis AM, Golokhvast KS.
849 Characterization of fume particles generated during arc welding with various covered electrodes. Sci Rep. 2018
850 21;8(1): 17169.
851 Krishnaraj J, Kowshik J, Sebastian R, Raghavan SC, Nagini S. Exposure to welding fumes activates DNA damage
852 response and redox-sensitive transcription factor signalling in Sprague-Dawley rats. Toxicol Lett. 2017 274: 8-
853 19.
854 Krishnaraj J, Baba AB, Viswanathan P, Veeravarmal V, Balasubramanian V, Nagini S. Impact of stainless-steel
855 welding fumes on proteins and non-coding RNAs regulating DNA damage response in the respiratory tract of
856 Sprague-Dawley rats. J Toxicol Environ Health A. 2018 81(24):1231-1245.
857 Leclercq B, Happillon M, Antherieu S, Hardy EM, Alleman LY, Grova N, Perdrix E, Appenzeller BM, Lo Guidice
858 JM, Coddeville P, Garçon G. Differential responses of healthy and chronic obstructive pulmonary diseased
859 human bronchial epithelial cells repeatedly exposed to air pollution-derived PM_4. Environ Pollut. 2016 218:
860 1074-1088.
861 Leclercq, B., Alleman, L.Y., Perdrix, E., Riffault, V., Happillon, M., Strecker, A., Lo-Guidice, J.M., Garçon, G.,
862 Coddeville, P. Particulate metal bioaccessibility in physiological fluids and cell culture media: Toxicological
863 perspectives. Environ Res. 2017a 156: 148-157.
864 Leclercq B, Platel A, Antherieu S, Alleman LY, Hardy EM, Perdrix E, Grova N, Riffault V, Appenzeller BM,
865 Happillon M, Nesslany F, Coddeville P, Lo-Guidice JM, Garçon G. Genetic and epigenetic alterations in
866 normal and sensitive COPD-diseased human bronchial epithelial cells repeatedly exposed to air pollution-
867 derived $PM_{2.5}$. Environ Pollut. 2017b 230:163-177.
868 Leclercq B, Kluza J, Antherieu S, Sotty J, Alleman LY, Perdrix E, Loyens A, Coddeville P, Lo Guidice JM,
869 Marchetti P, Garçon G. Air pollution-derived $PM_{2.5}$ impairs mitochondrial function in healthy and chronic
870 obstructive pulmonary diseased human bronchial epithelial cells. Environ Pollut. 2018 243(Pt B):1434-1449.
871 Leonard SS, Chen BT, Stone SG, Schwegler-Berry D, Kenyon AJ, Frazer D, Antonini JM. Comparison of stainless
872 and mild steel welding fumes in generation of reactive oxygen species. Part Fibre Toxicol. 2010 7: 32.
873 Leso V, Vetrani I, Della Volpe I, Nocera C, Iavicoli I. Welding Fume Exposure and Epigenetic Alterations: A
874 Systematic Review. Int J Environ Res Public Health. 2019 16(10): 1745.
875 Li J, Li WX, Bai C, Song Y. Particulate matter-induced epigenetic changes and lung cancer. Clin Respir J. 2017
876 11(5): 539-546.
877 Longhin E, Pezzolato E, Mantecca P, Holme JA, Franzetti A, Camatini M, Gualtieri M. Season linked responses to
878 fine and quasi-ultrafine Milan PM in cultured cells. Toxicol in vitro 2013 27: 551-559.

879 Longhin E, Capasso L, Battaglia C, Proverbio MC, Consentino C, Cifola I, Mangano E, Camatini M, Gualtieri M
880 Integrative transcriptomic and protein analysis of human bronchial BEAS-2B exposed to seasonal urban
881 particulate matter. Environ Pollut. 2016 209: 87-98.
882 Longhin E, Holme JA, Gualtieri M, Camatini M, Øvrevik J. Milan winter fine particulate matter ($wPM_{2.5}$) induces
883 IL-6 and IL-8 synthesis in human bronchial BEAS-2B cells, but specifically impairs IL-8 release. Toxicol In
884 Vitro. 2018 52: 365-373.
885 Lovell, D.P., Omori, T. Statistical issues in the use of the comet assay. Mutagenesis 2008. 23, 171–182.
886 Marongiu A, Hasan O, Ali A, Bakhsh S, George B, Irfan N, Minelli C, Canova C, Schofield S, De Matteis S,
887 Cullinan P. Are welders more at risk of respiratory infections? Findings from a cross-sectional survey and
888 analysis of medical records in shipyard workers: the WELSHIP project. Thorax. 2016 71(7): 601-6.
889 Mbengue S, Alleman LY, Flament P. Size-distributed metallic elements in submicronic and ultrafine atmospheric
890 particles from urban and industrial areas in northern France. Atmos Res 2014 135-136: 35-47.
891 McCarrick S, Wei Z, Moelijker N, Derr R, Persson KA, Hendriks G, Odnevall Wallinder I, Hedberg Y, Karlsson
892 HL. High variability in toxicity of welding fume nanoparticles from stainless steel in lung cells and reporter cell
893 lines: the role of particle reactivity and solubility. Nanotoxicology. 2019 13(10): 1293-1309.
894 MétroPol. MétroPol M-43 Chrome VI. 2016. Available online :
895 http://www.inrs.fr/publications/bdd/metropol/fiche.html?refINRS=METROPOL_43.
896 Oh JH, Yang MJ, Heo JD, Yang YS, Park HJ, Park SM, Kwon MS, Song CW, Yoon S, Yu IJ. Inflammatory
897 response in rat lungs with recurrent exposure to welding fumes: a transcriptomic approach. Toxicol Ind Health.
898 2012 28(3): 203-15.
899 Pega F, Chartres N, Guha N, Modenese A, Morgan RL, Martínez-Silveira MS, Loomis D. The effect of
900 occupational exposure to welding fumes on trachea, bronchus and lung cancer: A protocol for a systematic
901 review and meta-analysis from the WHO/ILO Joint Estimates of the Work-related Burden of Disease and
902 Injury. Environ Int. 2020 145: 106089.
903 Ren J, Li X, Dong H, Suo L, Zhang J, Zhang L, Zhang J. miR-210-3p regulates the proliferation and apoptosis of
904 non-small cell lung cancer cells by targeting SIN3A. Exp Ther Med. 2019 18(4): 2565-2573.
905 Saint-Georges F, Abbas I, Billet S, Verdin A, Gosset P, Mulliez P, Shirali P, Garçon G. Gene expression induction
906 of volatile organic compound and/or polycyclic aromatic hydrocarbon-metabolizing enzymes in isolated human
907 alveolar macrophages in response to airborne particulate matter ($PM_{2.5}$). Toxicology. 2008 244(2-3): 220-30.
908 Saleh Y, Antherieu S, Dusautoir R, Y Alleman L, Sotty J, De Sousa C, Platel A, Perdrix E, Riffault V, Fronval I,
909 Nesslany F, Canivet L, Garçon G, Lo-Guidice JM. Exposure to Atmospheric Ultrafine Particles Induces Severe
910 Lung Inflammatory Response and Tissue Remodeling in Mice. Int J Environ Res Public Health. 2019 16(7):
911 1210.
912 Samulin Erdem J, Arnoldussen YJ, Tajik S, Ellingsen DG, Zienolddiny S. Effects of mild steel welding fume
913 particles on pulmonary epithelial inflammation and endothelial activation. Toxicol Ind Health. 2020 36(12):
914 995-1001.
915 Shoeb M, Kodali VK, Farris BY, Bishop LM, Meighan TG, Salmen R, Eye T, Friend S, Schwegler-Berry D,
916 Roberts JR, Zeidler-Erdely PC, Erdely A, Antonini JM. Oxidative Stress, DNA Methylation, and Telomere

Length Changes in Peripheral Blood Mononuclear Cells after Pulmonary Exposure to Metal-Rich Welding Nanoparticles. NanoImpact. 2017 5: 61-69.

Singh, N.P., McCoy, M.T., Tice, R.R., Schneider, E.L. A simple technique for quantitation of low levels of DNA damage in individual cells. Exp Cell Res 1988 175: 184–191.

Smith CC, O'Donovan MR, Martin EA. hOGG1 recognizes oxidative damage using the comet assay with greater specificity than FPG or ENDOIII. Mutagenesis. 2006 21(3): 185-90.

Sotty J, Garçon G, Denayer FO, Alleman LY, Saleh Y, Perdrix E, Riffault V, Dubot P, Lo-Guidice JM, Canivet L. Toxicological effects of ambient fine ($PM_{2.5-0.18}$) and ultrafine ($PM_{0.18}$) particles in healthy and diseased 3D organo-typic mucocilary-phenotype models. Environ Res. 2019 176: 108538.

Sotty J, Kluza J, De Sousa C, Tardivel M, Anthérieu S, Alleman LY, Canivet L, Perdrix E, Loyens A, Marchetti P, Lo Guidice JM, Garçon G. Mitochondrial alterations triggered by repeated exposure to fine ($PM_{2.5-0.18}$) and quasi-ultrafine ($PM_{0.18}$) fractions of ambient particulate matter. Environ Int. 2020 142: 105830.

Stanislawska M, Janasik B, Kuras R, Malachowska B, Halatek T, Wasowicz W. Assessment of occupational exposure to stainless steel welding fumes - A human biomonitoring study. Toxicol Lett. 2020 329: 47-55.

Stone V, Miller MR, Clift MJD, Elder A, Mills NL, Møller P, Schins RPF, Vogel U, Kreyling WG, Alstrup Jensen K, Kuhlbusch TAJ, Schwarze PE, Hoet P, Pietroiusti A, De Vizcaya-Ruiz A, Baeza-Squiban A, Teixeira JP, Tran CL, Cassee FR. Nanomaterials Versus Ambient Ultrafine Particles: An Opportunity to Exchange Toxicology Knowledge. Environ Health Perspect. 2017 125(10): 106002.

Tantawy MA, Shaheen S, Kattan SW, Alelwani W, Barnawi IO, Elmgeed GA, Nafie MS. Cytotoxicity, *in silico*predictions and molecular studies for androstane heterocycle compounds revealed potential antitumor agent against lung cancer cells. J Biomol Struct Dyn. 2020 10: 1-14.

Tice RR, Agurell E, Anderson D, Burlinson B, Hartmann A, Kobayashi H, Miyamae Y, Rojas E, Ryu JC, Sasaki YF. Single cell gel/comet assay: guidelines for in vitro and in vivo genetic toxicology testing. Environ. Mol. Mutagen. 2000. 35: 206-21.

Tice, R.R., Agurell, E., Anderson, D., Burlinson, B., Hartmann, A., Kobayashi, H., Miyamae, Y., Rojas, E., Ryu, J.-C., Sasaki, Y.F. Single cell gel/comet assay: Guidelines for in vitro and in vivo genetic toxicology testing. Environ. Mol. Mut. 2000 35: 206–221.

Tungsukruthai S, Reamtong O, Roytrakul S, Sukrong S, Vinayanwattikun C, Chanvorachote P. Targeting AKT/mTOR and Bcl-2 for Autophagic and Apoptosis Cell Death in Lung Cancer: Novel Activity of a Polyphenol Compound. Antioxidants (Basel). 2021 10(4): 534.

Veranth, J.M.; Kaser, E.G.; Veranth, M.M.; Koch, M.; Yost, G.S. Cytokine responses of human lung cells (BEAS-2B) treated with micron-sized and nanoparticles of metal oxides compared to soil dusts. Part. Fibre Toxicol. 2007, 4: 2.

Vrijens K, Bollati V, Nawrot TS. MicroRNAs as potential signatures of environmental exposure or effect: a systematic review. Environ Health Perspect. 2015 123: 399-411.

Wardyn JD, Ponsford AH, Sanderson CM. Dissecting molecular cross-talk between Nrf2 and NF-κB response pathways. Biochem Soc Trans. 2015 43(4): 621-6.

954 Welding, molybdenum trioxide, and indium tin oxide / IARC Working Group on the Evaluation of Carcinogenic
955 Risks to Humans (2017: Lyon, France) (IARC monographs on the evaluation of carcinogenic risks to humans;
956 volume 118) I. International Agency for Research on Cancer II. Series ISBN 978-92-832-0185-4 (NLM
957 Classification: W1) ISSN 1017-1606 pp33-266.
958 Witte, I., Plappert, U., de Wall, H., Hartmann, A., Genetic Toxicity Assessment: Employing the Best Science for
959 Human Safety Evaluation Part III: The Comet Assay as an Alternative to In Vitro Clastogenicity Tests for Early
960 Drug Candidate Selection. Toxicol. Sci. 2007 97: 21–26.
961 Xu X, Wells A, Padilla MT, Kato K, Kim KC, Lin Y. A signaling pathway consisting of miR-551b, catalase and
962 MUC1 contributes to acquired apoptosis resistance and chemoresistance. Carcinogenesis. 2014 35(11): 2457-
963 66.
964 Yildirim M, Oztay F, Kayalar O, Tasci AE. Effect of long noncoding RNAs on epithelial-mesenchymal transition
965 in A549 cells and fibrotic human lungs. J Cell Biochem. 2021 doi: 10.1002/jcb.29920. Epub ahead of print.
966 PMID: 33847014.
967 Zeidler-Erdely PC, Kashon ML, Li S, Antonini JM. Response of the mouse lung transcriptome to welding fume:
968 effects of stainless and mild steel fumes on lung gene expression in A/J and C57BL/6J mice. Respir Res. 2010
969 11(1): 70.
970 Zeidler-Erdely PC, Kashon ML, Li S, Antonini JM. Response of the mouse lung transcriptome to welding fume:
971 effects of stainless and mild steel fumes on lung gene expression in A/J and C57BL/6J mice. Respir Res. 2010
972 11(1): 70.
973 Zeidler-Erdely PC, Falcone LM, Antonini JM. Influence of welding fume metal composition on lung toxicity and
974 tumor formation in experimental animal models. J Occup Environ Hyg. 2019 16(6): 372-377.
975 Zheng W, Antonini JM, Lin YC, Roberts JR, Kashon ML, Castranova V, Kan H. Cardiovascular effects in rats
976 after intratracheal instillation of metal welding particles. Inhal Toxicol. 2015 27(1): 45-53.
977

TABLES

980 **Table 1: Elements and oxides within welding fumes-derived quasi-ultrafine particles**

ELEMENT [#]	MW (g/mol)	Concentration (ng/µg)	OXIDE[1]	MW (g/mol)	Concentration (ng/µg)	Proportion (%)
Al	27.0	1.5	Al_2O_3	102.0	2.8	0.3%
Ca	40.1	7.6	CaO	56.1	10.7	1.1%
Cr	52.0	129.4	Cr_2O_3	152.0	189.1	20.0%
Cu	63.5	4.0	CuO	79.5	5.0	0.5%
Fe	55.8	259.8	Fe_2O_3	159.7	371.4	39.4%
K	39.1	1.2	K_2O	94.2	1.4	0.1%
Mg	24.3	0.9	MgO	40.3	1.5	0.2%
Mn	54.9	127.6	MnO	70.9	164.7	17.5%
Mo	95.9	13.1	MoO_3	143.9	19.7	2.1%
Na	23.0	1.5	Na_2O	62.0	2.1	0.2%
Ni	58.7	43.2	NiO	74.7	54.9	5.8%
Si	28.1	55.6	SiO_2	60.1	118.9	12.6%
Zn	65.4	1.4	ZnO	81.4	1.8	0.2%
Total		646.9			944.0	100%

981 [#] refers to the most likely main metal oxide in welding fumes (> 1 ng/µg).
982

983 **FIGURE LEGEND**

984

985 **Figure 1:** ATP concentrations in normal human bronchial epithelial BEAS-2B cells 24 h after one (Figure 1-A) or
986 three (Figure 1-B) 24 h-exposures to increasing concentrations (i.e., ranging from 0.1 to 50 µg/cm²) of the quasi-
987 ultrafine particle (Q-UFP) fraction of welding fumes emitted by gas metal arc welding-stainless steel. As indicated
988 by the red black dotted lines on Figure 1-A and 1-B, respectively, the lowly- (i.e., lethal concentration at 10 %, LC_{10})
989 and highly (i.e., lethal concentration at 40 %, LC_{40})-cytotoxic doses of 1.5 and 9 µg/cm² were used for the acute
990 scenario of exposure, and the lowly- (i.e., LC_{10}) and highly (i.e., LC_{40})-cytotoxic doses of 0.25 and 1.5 µg/cm² were
991 used for the repeated scenario of exposure, in order to further investigate the other toxicological endpoints under
992 study. Values are depicted as means and standard deviations (n = 5). (Student t-test versus negative controls: *: $p <$
993 0.05; ***: $p < 0.001$).

994

995 **Figure 2:** Chloromethyl derivative of 2',7'-dichlorodihydrofluorescein diacetate (CM-H_2DCFDA) fluorescence
996 (Figure 2-A), binding activity of nuclear factor erythroid 2 p45-related factor 2 (NRF2) to antioxidant response
997 elements (ARE) (Figure 2-B), and NRF2 target gene expression (i.e., heme oxygenase: HMOX and -NADPH
998 quinone oxido-reductase-1: NQO-1; Figures 2-C and 2-D) in normal human bronchial epithelial BEAS-2B cells 24 h
999 after one (white histogram bars) or three (grey histogram bars) 24 h-exposures to the quasi-ultrafine particle (Q-UFP)
1000 fraction of welding fumes emitted by gas metal arc welding-stainless steel. Values are depicted as means and
1001 standard deviations (n = 5). (Student t-test versus negative controls: *: $p < 0.05$; **: $p < 0.01$; ***: $p<0.001$).

1002

1003 **Figure 3:** Glutathione status (i.e. ratio between the oxidized and the reduced forms; Figure 3-A), 8-hydroxy-2'-
1004 deoxyguanosine (8-OHdG; Figure 3-B), carbonylated protein (CO-PROT; Figure 3-C), and 4-hydroxynonenal (4-
1005 HNE; Figure 3-D) in normal human bronchial epithelial BEAS-2B cells 24 h after one (white histogram bars) or
1006 three (grey histogram bars) 24 h-exposures to the quasi-ultrafine particle (Q-UFP) fraction of welding fumes emitted
1007 by gas metal arc welding-stainless steel. Values are depicted as means and standard deviations (n = 5). (Student t-test
1008 versus negative controls: *: $p < 0.05$; **: $p < 0.01$; ***: $p < 0.001$).

1009

1010 **Figure 4:** Binding activity of nuclear factor-kappa B (NF-κB) to DNA κB motifs (Figure 2-A), and tumor necrosis
1011 factor-alpha (TNF-α), Interleukin-1 beta (IL-1β) and interleukin-6 (IL-6) gene expression (Figure 4-B, 4-D, and 4-F,
1012 respectively) and protein secretion (Figure 4-C, 4-E, and 4-G, respectively) in normal human bronchial epithelial
1013 BEAS-2B cells 24 h after one (white histogram bars) or three (grey histogram bars) 24 h-exposures to the quasi-
1014 ultrafine particle (Q-UFP) fraction of welding fumes emitted by gas metal arc welding-stainless steel. Values are
1015 depicted as means and standard deviations (n = 5). (Student t-test versus negative controls: **: $p < 0.01$; ***: $p <$
1016 0.001).

1017

1018 **Figure 5:** Primary DNA damage assessed with the alkaline comet assay in normal human bronchial epithelial
1019 BEAS-2B cells after 4 h, 24 h or 3 x 24 h (Figures 6-A, 6-B and 6-C, respectively) of exposure to the quasi-ultrafine

particle (Q-UFP) fraction of welding fumes emitted by gas metal arc welding-stainless steel. Both the standard (i.e., dark grey histogram bars) and the hOGG1-modified (i.e., slight grey histogram bars) comet assays were applied. Values are depicted as means of medians of % of tail intensity and standard deviations (n = 4). (Non-parametric Mann-Whitney U-test *versus* negative controls: *: $p < 0.05$). Cytotoxicity was assessed at harvest using the Trypan Blue dye exclusion assay. Results were expressed as percent of relative cell viability (i.e., the percent ratio of viable unstained cells to non-viable stained cells in exposed *versus* control groups).

Figure 6: Venn diagrams representing the differentially regulated genes down- and up-regulated (Figures 6-A and 6-B, respectively) in normal human bronchial epithelial BEAS-2B cells 24 h after one or three 24 h-exposures to the quasi-ultrafine particle (Q-UFP) fraction of welding fumes emitted by gas metal arc welding-stainless steel. (i.e., Fold-Change: FC > 1.5 or < 0.66, $p < 0.05$).

Figure 7: Histone deacetylase (HDAC) activity (Figure 7-A), histone acetyl transferase (HAT) activity (Figure 7-B), ratio between HDAC activity and HAT activity (HDAC/HAT; Figure 7-C), histone H3Lys27ac concentration (Figure 7-D), histone H3Lys9ac concentration (Figure 7-E), and DNA global methylation (Figure 7-F) in normal human bronchial epithelial BEAS-2B cells 24 h after one (white histogram bars) or three (grey histogram bars) 24 h-exposures to the quasi-ultrafine particle (Q-UFP) fraction of welding fumes emitted by gas metal arc welding-stainless steel. Values are depicted as means and standard deviations (n = 5). (Student t-test versus negative controls: *: $p < 0.05$; **: $p < 0.01$; ***: $p < 0.001$).

Figure 8: Venn diagrams representing the differentially regulated microRNA down- and up-regulated (Figures 8-A and 8-B, respectively) in normal human bronchial epithelial BEAS-2B cells 24 h after one or three 24 h-exposures to the quasi-ultrafine particle (Q-UFP) fraction of welding fumes emitted by gas metal arc welding-stainless steel. (i.e., Fold-Change: FC > 1.5 or < 0.66, $p < 0.05$).

Figure 9: Venn diagrams representing the target genes of differentially regulated microRNA (i.e., has-miR-331-5p, Figure 9-A; has-miR-210-3p, Figure 9-B; has-miR-424-5p, Figure 9-C; has-miR-597-5p, Figure 9-D; has-miR-212-3p, Figure 9-E; has-miR-1260a, Figure 9-F; has-miR-1248, Figure 9-G; has-miR-625-5p, Figure 9-H; has-miR-744-3p, Figure 9-I; and has-miR-755-3p, Figure 9-J), as assessed using TargetScanHuman v7.2 (http://www.targetscan.org/vert_72/), miRNA target Prediction Database (miRDB; http://mirdb.org), and DIANA TOOLS Tarbase V8 (http://carolina.imis.athena-innovation.gr/diana_tools/web/index.php?r=tarbasev8%2Findex), and crossed with differentially deregulated genes by quasi-ultrafine particle (Q-UFP) fraction of welding fumes emitted by gas metal arc welding-stainless steel.

Figure 10: Annexin V labelling (Figure 10-A) and activities of caspases 3/7, 8, and 9 (Figure 10-B, 10-C, and 10-D, respectively), in normal human bronchial epithelial BEAS-2B cells 24 h after one (white histogram bars) or three (grey histogram bars) 24 h-exposures to the quasi-ultrafine particle (Q-UFP) fraction of welding fumes emitted by

1057 gas metal arc welding-stainless steel. Values are depicted as means and standard deviations (n = 5). (Student t-test
1058 versus negative controls: *: $p<0.05$; **: $p<0.01$; ***: $p<0.001$).
1059

A

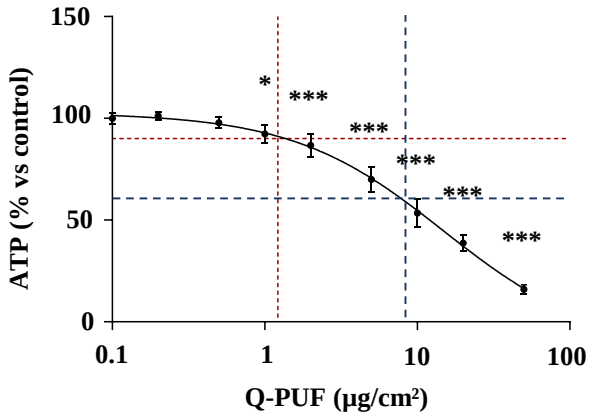
150
100
50
0
ATP (% vs control)
*
***
***
***
***
***
0.1
1
10
100
Q-PUF (µg/cm²)

B

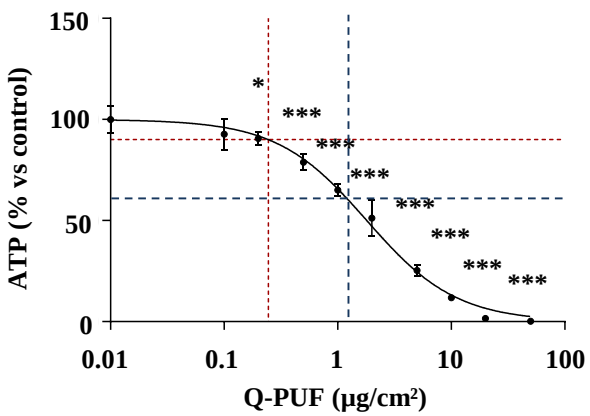
150
100
50
0
ATP (% vs control)
*
***
***
***
***
***
***
0.01
0.1
1
10
100
Q-PUF (µg/cm²)

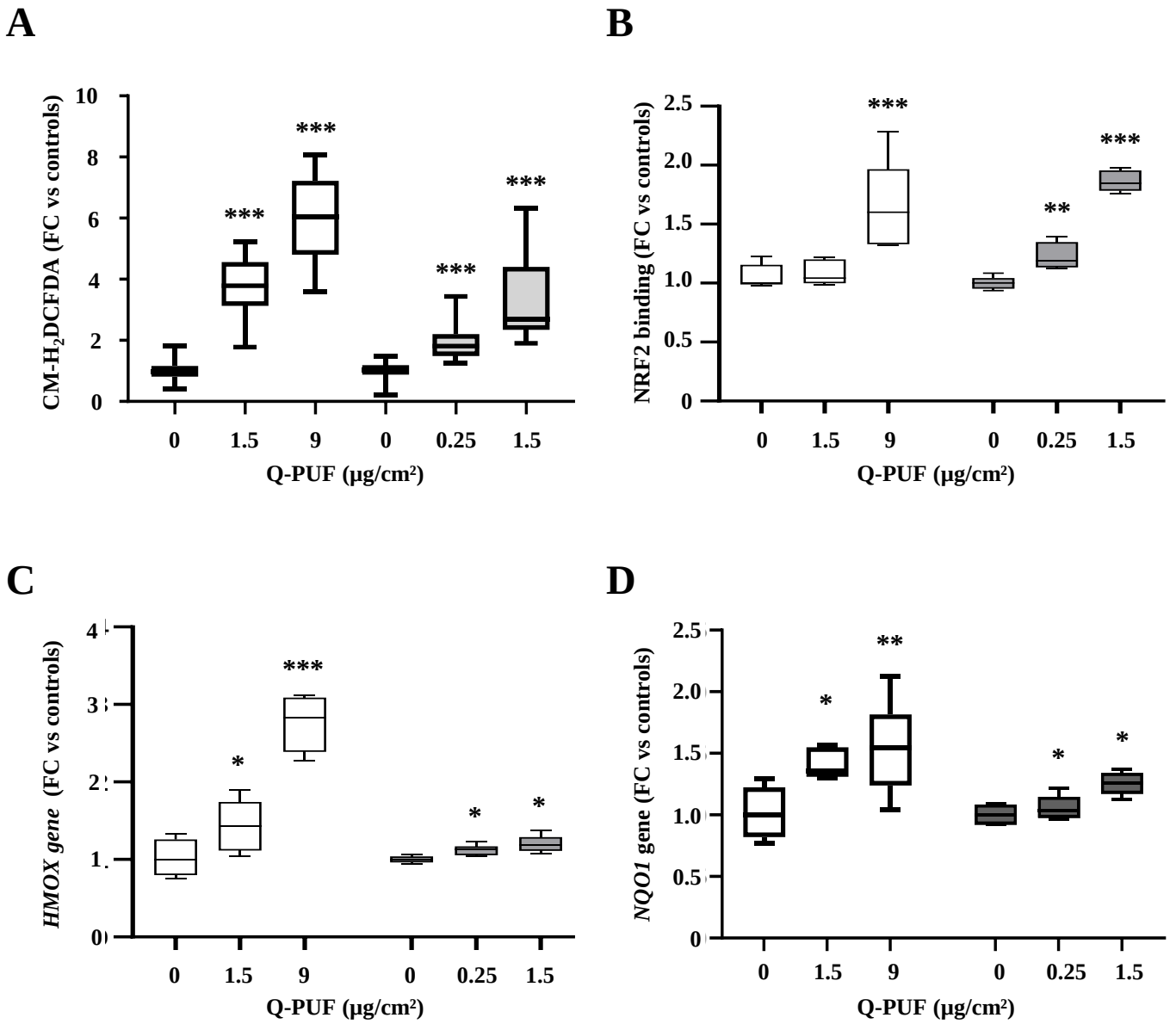
A
CM-H2DCFDA (FC vs controls)
10
8
6
4
2
0
***
***
***
***
0
1.5
9
0
0.25
1.5
Q-PUF (µg/cm²)
B
NRF2 binding (FC vs controls)
2.5
2.0
1.5
1.0
0.5
0
***
**
***
0
1.5
9
0
0.25
1.5
Q-PUF (µg/cm²)
C
HMOX gene (FC vs controls)
4
3
2
1
0
*
***
*
*
0
1.5
9
0
0.25
1.5
Q-PUF (µg/cm²)
D
NQO1 gene (FC vs controls)
2.5
2.0
1.5
1.0
0.5
0
*
**
*
*
0
1.5
9
0
0.25
1.5
Q-PUF (µg/cm²)

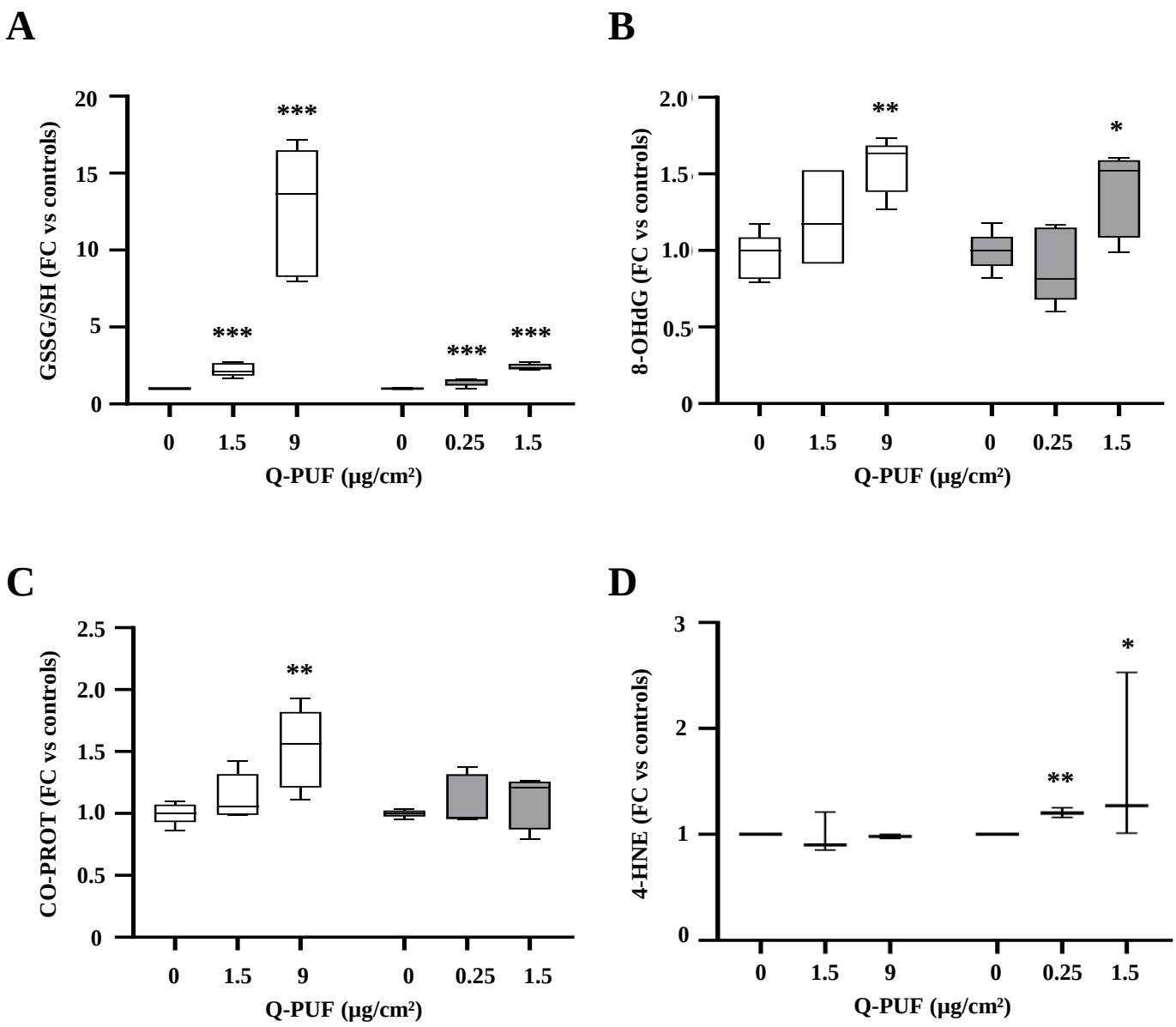
A
GSSG/SH (FC vs controls)
20
15
10
5
0
***
***
***
***
0
1.5
9
0
0.25
1.5
Q-PUF (µg/cm²)
B
8-OHdG (FC vs controls)
2.0
1.5
1.0
0.5
0
**
*
0
1.5
9
0
0.25
1.5
Q-PUF (µg/cm²)
C
CO-PROT (FC vs controls)
2.5
2.0
1.5
1.0
0.5
0
**
0
1.5
9
0
0.25
1.5
Q-PUF (µg/cm²)
D
4-HNE (FC vs controls)
3
2
1
0
**
*
0
1.5
9
0
0.25
1.5
Q-PUF (µg/cm²)

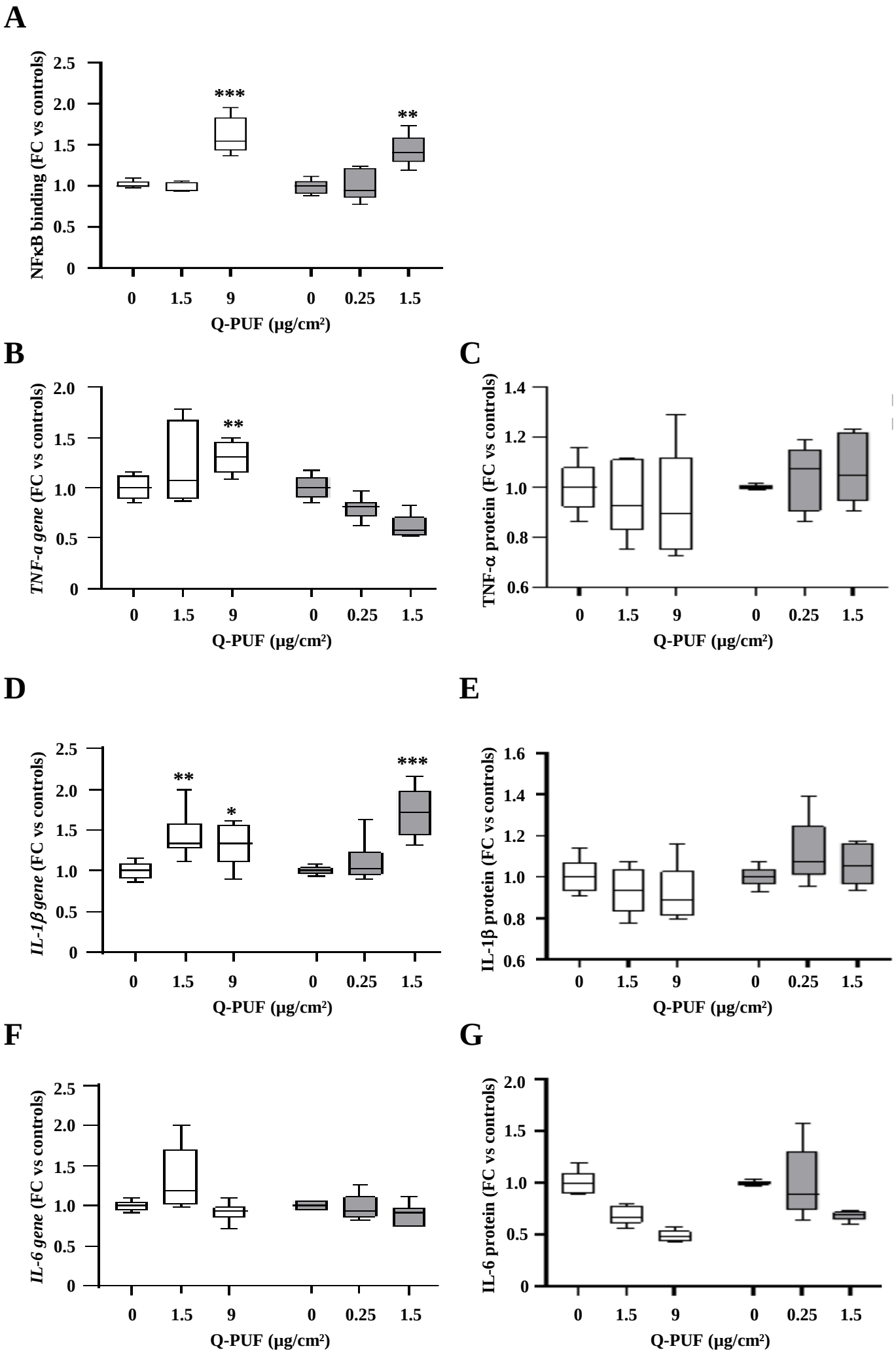
A
NFκB binding (FC vs controls)
2.5
2.0
1.5
1.0
0.5
0
***
**
0
1.5
9
0
0.25
1.5
Q-PUF (µg/cm²)
B
TNF-a gene (FC vs controls)
2.0
1.5
1.0
0.5
0
**
0
1.5
9
0
0.25
1.5
Q-PUF (µg/cm²)
C
TNF-α protein (FC vs controls)
1.4
1.2
1.0
0.8
0.6
0
1.5
9
0
0.25
1.5
Q-PUF (µg/cm²)
D
IL-1β gene (FC vs controls)
2.5
2.0
1.5
1.0
0.5
0
**
*
***
0
1.5
9
0
0.25
1.5
Q-PUF (µg/cm²)
E
IL-1β protein (FC vs controls)
1.6
1.4
1.2
1.0
0.8
0.6
0
1.5
9
0
0.25
1.5
Q-PUF (µg/cm²)
F
IL-6 gene (FC vs controls)
2.5
2.0
1.5
1.0
0.5
0
0
1.5
9
0
0.25
1.5
Q-PUF (µg/cm²)
G
IL-6 protein (FC vs controls)
2.0
1.5
1.0
0.5
0
0
1.5
9
0
0.25
1.5
Q-PUF (µg/cm²)

A

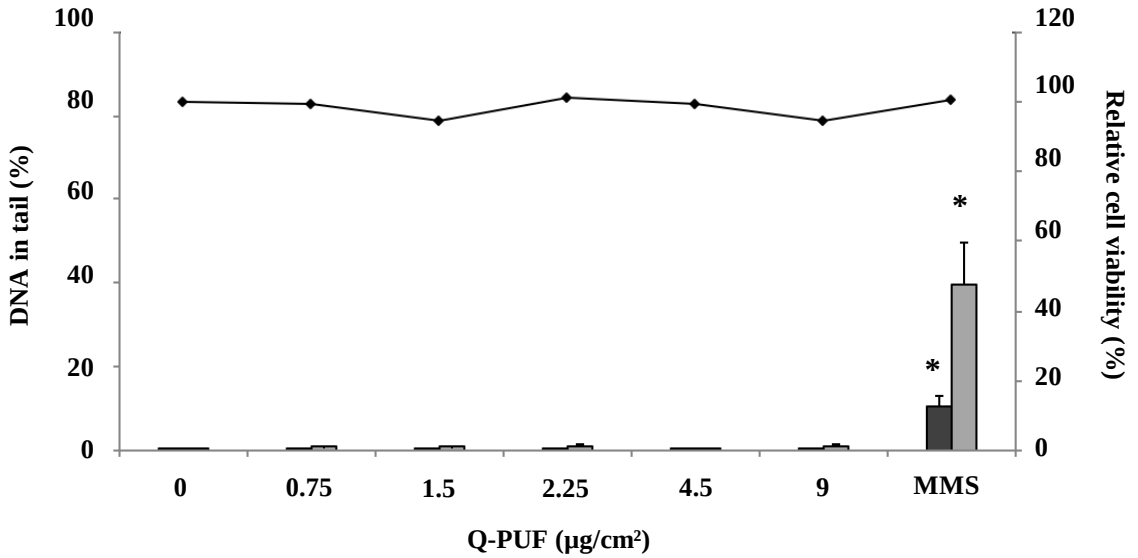
100
80
60
40
20
0
120
100
80
60
40
20
0
DNA in tail (%)
Relative cell viability (%)
*
*
0
0.75
1.5
2.25
4.5
9
MMS
Q-PUF (µg/cm²)

B

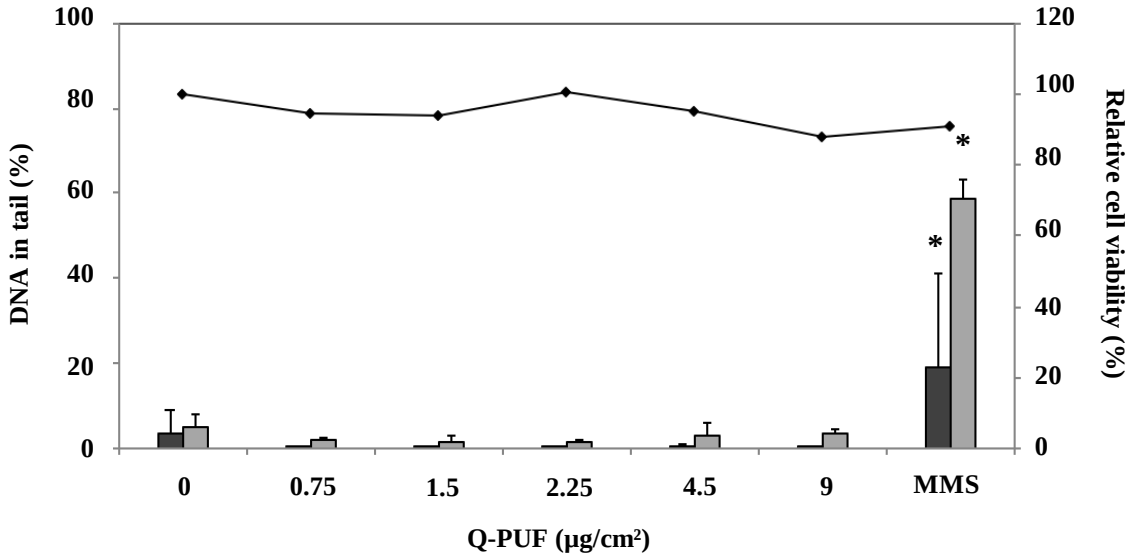
100
80
60
40
20
0
120
100
80
60
40
20
0
DNA in tail (%)
Relative cell viability (%)
*
*
0
0.75
1.5
2.25
4.5
9
MMS
Q-PUF (µg/cm²)

C

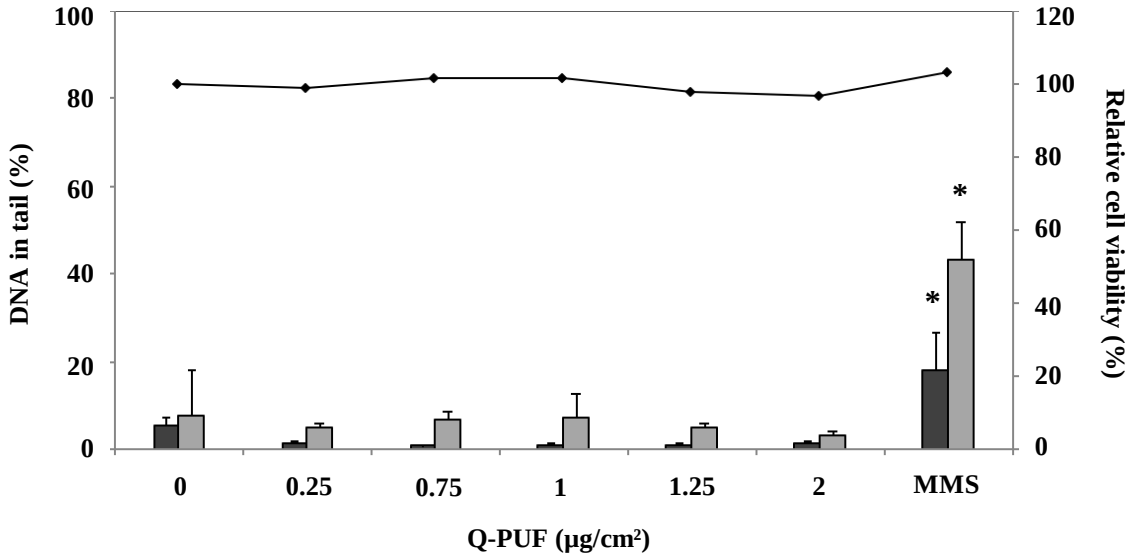
100
80
60
40
20
0
120
100
80
60
40
20
0
DNA in tail (%)
Relative cell viability (%)
*
*
0
0.25
0.75
1
1.25
2
MMS
Q-PUF (µg/cm²)

A

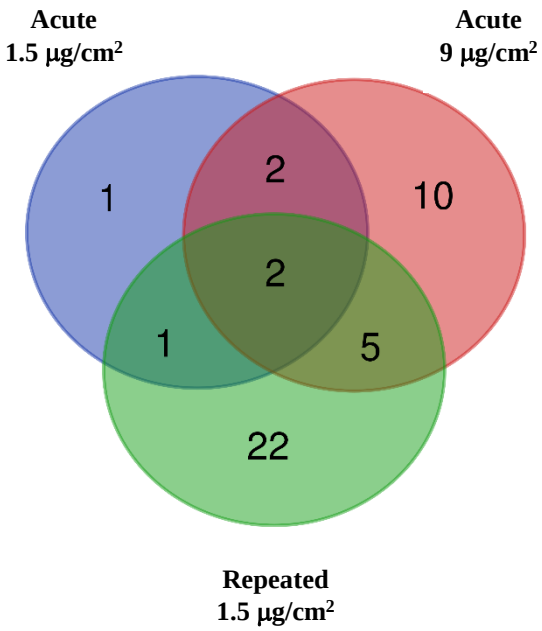

B

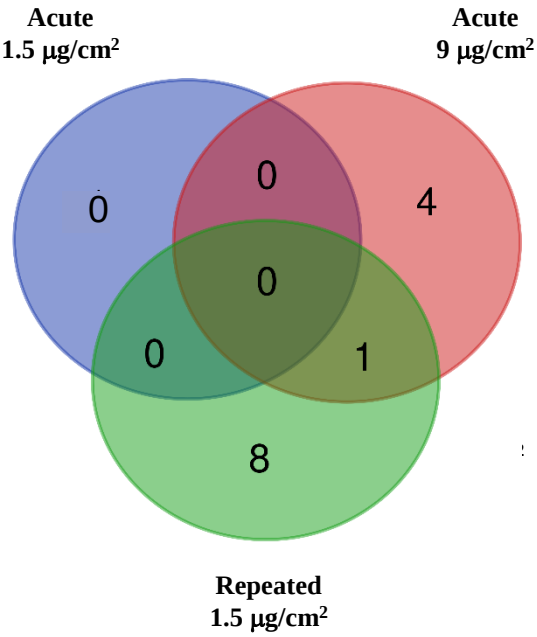

Exposure/Dose (µg/cm²)	Down-regulated genes
Acute 1.5 µg/cm² Acute 9 µg/cm² Repeated 1.5 µg/cm²	*CDK4, MTOR*
Acute 1.5 µg/cm² Acute 9 µg/cm²	*HSPD1, RHEB*
Acute 1.5 µg/cm² Repeated 1.5 µg/cm²	*RHEB*
Acute 9 µg/cm² Repeated 1.5 µg/cm²	*JAK2, HMBS, LEF1, BCL2, PENK*
Acute 1.5 µg/cm²	*SMAD4*
Acute 9 µg/cm²	*PP3CA, IKBKG, AREG, MYD88, PPARG, MAP3K7, CASP1, RASA1, TCF7, NCAM1*
Repeated 1.5 µg/cm²	*LPAR2, CCNB1, TLR4, TLR6, MAP4K1, CDKN2A, GALR2, HSPA5, NKD1, CALCRL, IL12A, MAPKAPK3, SCL44A2, KSR1, GATA3, ODC1, WISP3, MEF2C, SOXS2, WNT5B, ADORA1, INHA*

Exposure/Dose (µg/cm²)	Up-regulated genes
Acute 9 µg/cm² Repeated 1.5 µg/cm²	*PDK1*
Acute 1.5 µg/cm²	-
Acute 9 µg/cm²	*HMOX1, FOSB, MAP4K1, MYC*
Repeated 1.5 µg/cm²	*FZD8, CCL20, HK2, ENO2, GAPDH, IL8, CSF2, GYS1*

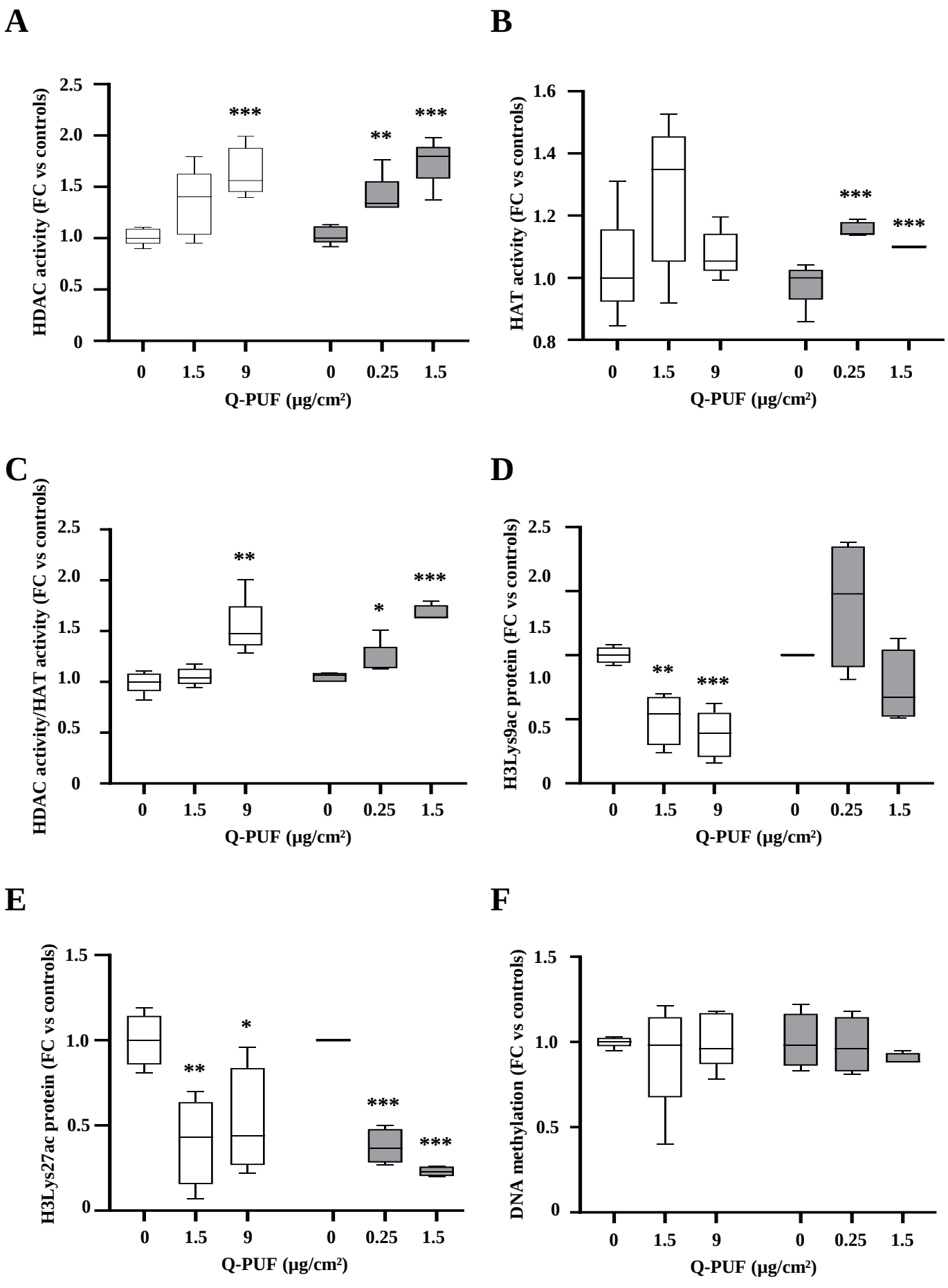
A
HDAC activity (FC vs controls)
2.5
2.0
1.5
1.0
0.5
0
***
**
***
0
1.5
9
0
0.25
1.5
Q-PUF (µg/cm²)
B
HAT activity (FC vs controls)
1.6
1.4
1.2
1.0
0.8
***
***
0
1.5
9
0
0.25
1.5
Q-PUF (µg/cm²)
C
HDAC activity/HAT activity (FC vs controls)
2.5
2.0
1.5
1.0
0.5
0
**
*
***
0
1.5
9
0
0.25
1.5
Q-PUF (µg/cm²)
D
H3Lys9ac protein (FC vs controls)
2.5
2.0
1.5
1.0
0.5
0
**
***
0
1.5
9
0
0.25
1.5
Q-PUF (µg/cm²)
E
H3Lys27ac protein (FC vs controls)
1.5
1.0
0.5
0
**
*
***
***
0
1.5
9
0
0.25
1.5
Q-PUF (µg/cm²)
F
DNA methylation (FC vs controls)
1.5
1.0
0.5
0
0
1.5
9
0
0.25
1.5
Q-PUF (µg/cm²)

A

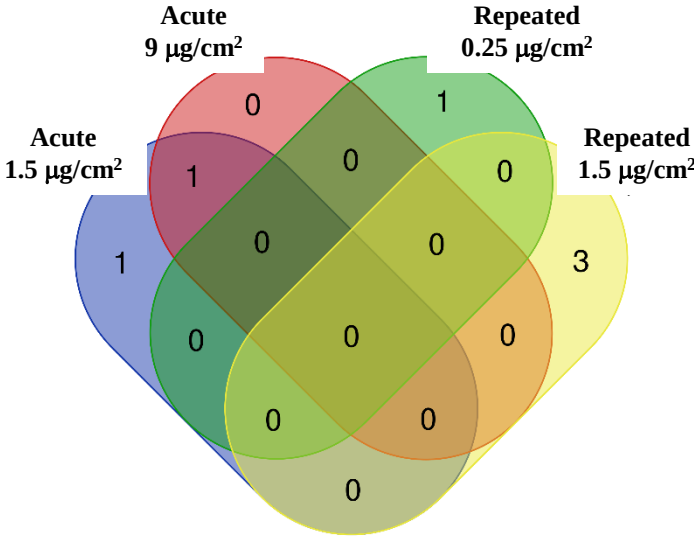

B

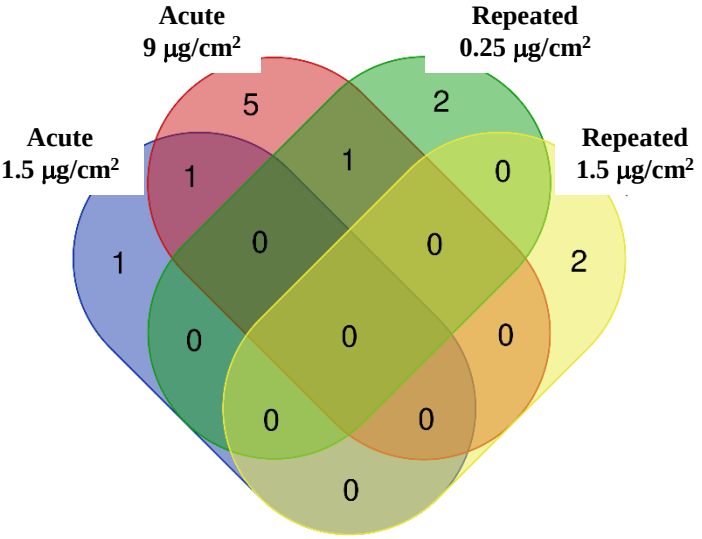

Exposure/Dose (µg/cm²)	Down-regulated miR
Acute 1.5 µg/cm² Acute 9 µg/cm²	hsa-miR-551b#
Acute 1.5 µg/cm²	hsa-miR-92a-3p
Repeated 0.25 µg/cm²	hsa-miR-548-3p
Repeated 1.5 µg/cm²	hsa-miR-1233, hsa-miR-339-3p, hsa-miR-378a-5p

Exposure/Dose (µg/cm²)	Up-regulated miR
Acute 1.5 µg/cm² Acute 9 µg/cm²	hsa-miR-331-5p
Acute 9 µg/cm² Repeated 0.25 µg/cm²	hsa-miR-210-3p
Acute 1.5 µg/cm²	hsa-miR-424-5p
Acute 9 µg/cm²	hsa-miR-597-5p, hsa-miR-212-3p, hsa-miR-1260a, hsa-miR-1248, hsa-miR-625-5p
Repeated 0.25 µg/cm²	hsa-miR-494-3p, hsa-miR-1274b
Repeated 1.5 µg/cm²	hsa-miR-744-3p, hsa-miR-766-3p

A – hsa-miR-331-5p

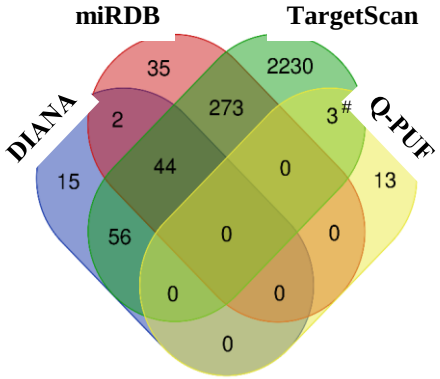

#*BCL2, JAK2, SMAD4*

B – hsa-miR-210-3p

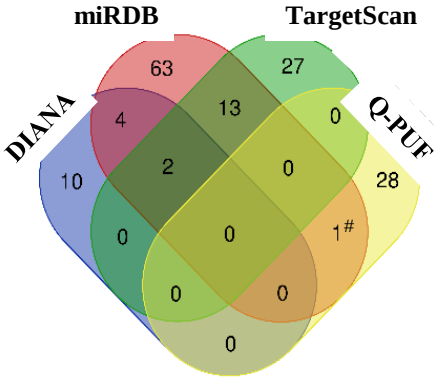

#*GALR2*

C – hsa-miR-424-5p

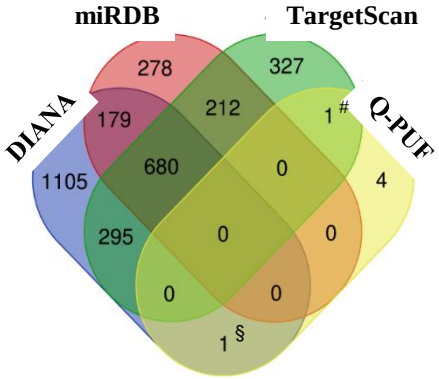

#CDK4 §SMAD4

D – hsa-miR-597-5p

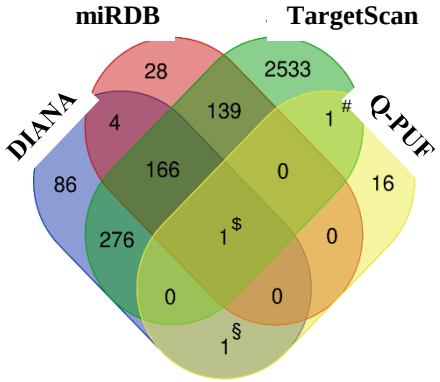

#*IKBKG* §*PPARG* $*NCAM1*

E – hsa-miR-212-3p

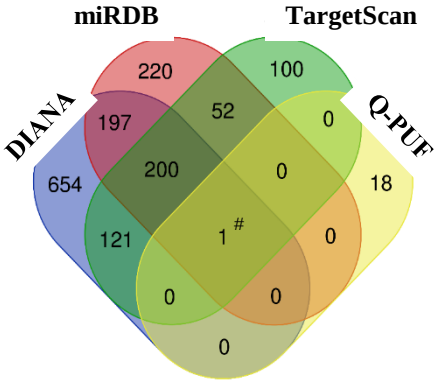

#*RASA1*

F – hsa-miR-1260a

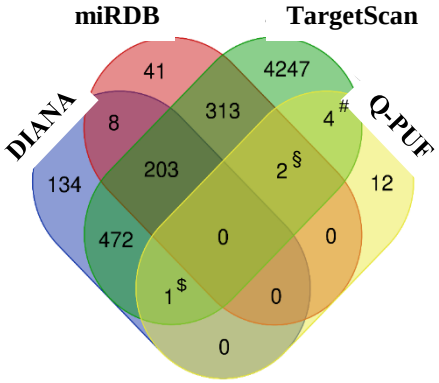

#*BCL2, RASA1, CASP1, MYD88*
§*TCF7, PENK* $*IKBKG*

G – hsa-miR-1248

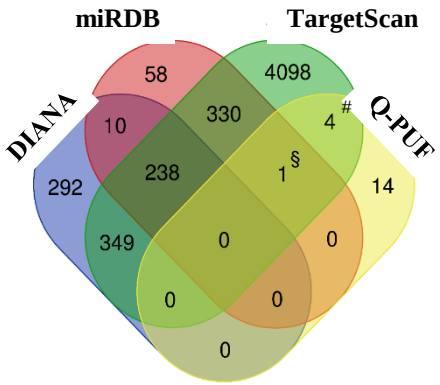

#*IMAP3K7, CDK4, IKBKG, MYD88*
§*BCL2*

H – hsa-miR-625-5p

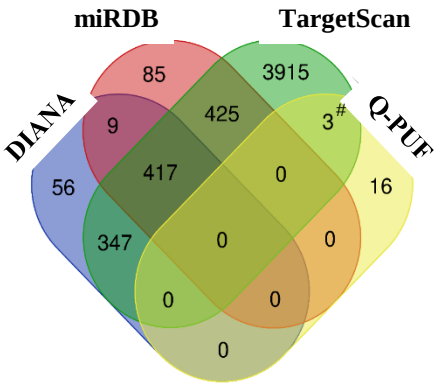

#*TCF7, IKBKG, CDK4*

I – hsa-miR-744-3p

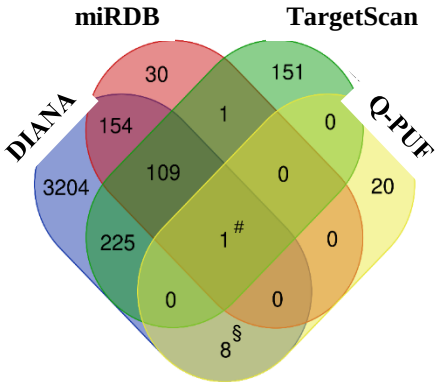

#*MEF2C* §*NKD1, BCL2, CDK4, TLR6, LEF1, LPAR2, ADORA1, CALCRL*

J – hsa-miR-766-3p

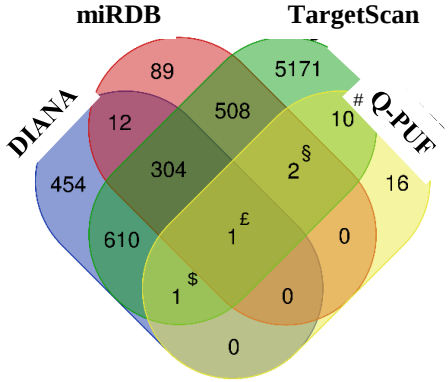

#*CCNB1, BCL2, STAT5A, MEF2C, LPAR2, TLR4, NKD1, SLC44A2, TLR6, CALCRL*
§*LEF1, WNT5B* $*KSR1* £*ADORA1*

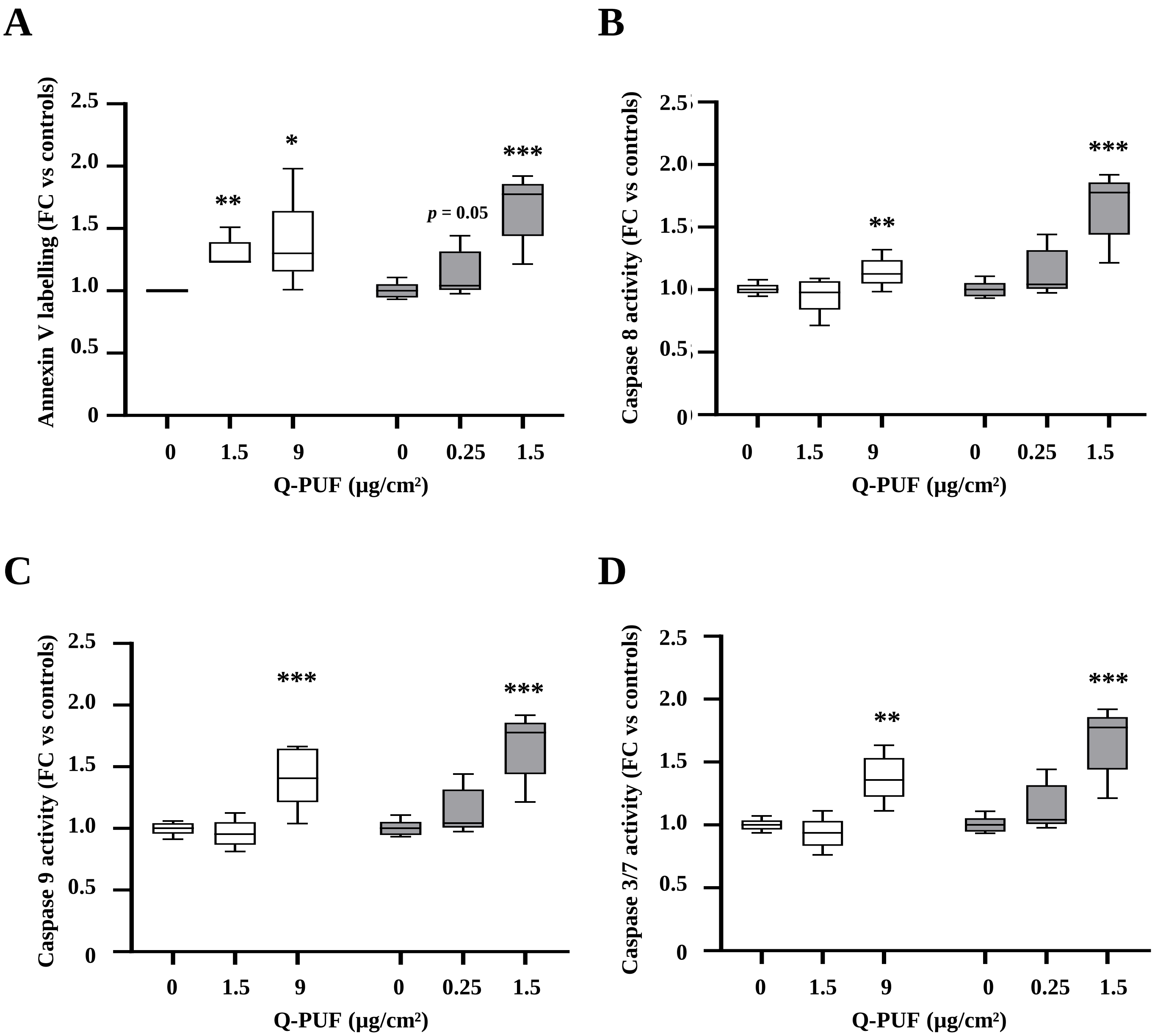
A
Annexin V labelling (FC vs controls)
2.5
2.0
1.5
1.0
0.5
0
**
*
p = 0.05
***
0
1.5
9
0
0.25
1.5
Q-PUF (µg/cm²)
B
Caspase 8 activity (FC vs controls)
2.5
2.0
1.5
1.0
0.5
0
**
***
0
1.5
9
0
0.25
1.5
Q-PUF (µg/cm²)
C
Caspase 9 activity (FC vs controls)
2.5
2.0
1.5
1.0
0.5
0
***
***
0
1.5
9
0
0.25
1.5
Q-PUF (µg/cm²)
D
Caspase 3/7 activity (FC vs controls)
2.5
2.0
1.5
1.0
0.5
0
**
***
0
1.5
9
0
0.25
1.5
Q-PUF (µg/cm²)

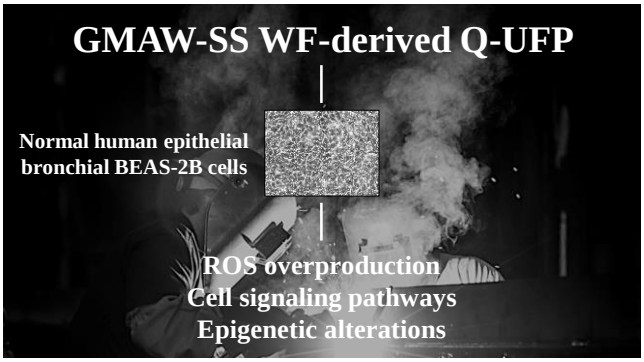
GMAW-SS WF-derived Q-UFP
Normal human epithelial bronchial BEAS-2B cells
ROS overproduction
Cell signaling pathways
Epigenetic alterations